Monthly Notices
of the
ROYAL ASTRONOMICAL SOCIETY

MNRAS **459,** 3596–3613 (2016)
Advance Access publication 2016 April 15

doi:10.1093/mnras/stw854

Kepler K2 observations of Sco X-1: orbital modulations and correlations with *Fermi* GBM and MAXI

Robert I. Hynes,[1]★ Bradley E. Schaefer,[1] Zachary A. Baum,[1] Ching-Cheng Hsu,[1] Michael L. Cherry[1] and Simone Scaringi[2]

[1]*Department of Physics and Astronomy, Louisiana State University, Baton Rouge, LA 70803, USA*
[2]*Max Planck Institute für Extraterrestriche Physik, D-85748 Garching, Germany*

Accepted 2016 April 12. Received 2016 March 16; in original form 2015 September 1

ABSTRACT

We present a multi-wavelength study of the low-mass X-ray binary Sco X-1 using *Kepler* K2 optical data and *Fermi* GBM and MAXI X-ray data. We recover a clear sinusoidal orbital modulation from the *Kepler* data. Optical fluxes are distributed bimodally around the mean orbital light curve, with both high and low states showing the same modulation. The high state is broadly consistent with the flaring branch of the Z-diagram and the low state with the normal branch. We see both rapid optical flares and slower dips in the high state, and slow brightenings in the low state. High-state flares exhibit a narrow range of amplitudes with a striking cut-off at a maximum amplitude. Optical fluxes correlate with X-ray fluxes in the high state, but in the low state they are anti-correlated. These patterns can be seen clearly in both flux–flux diagrams and cross-correlation functions and are consistent between MAXI and GBM. The high-state correlation arises promptly with at most a few minutes lag. We attribute this to thermal reprocessing of X-ray flares. The low-state anti-correlation is broader, consistent with optical lags of between zero and 30 min, and strongest with respect to high-energy X-rays. We suggest that the decreases in optical flux in the low state may reflect decreasing efficiency of disc irradiation, caused by changes in the illumination geometry. These changes could reflect the vertical extent or covering factor of obscuration or the optical depth of scattering material.

Key words: accretion, accretion discs – X-rays: binaries – X-rays: individual: Sco X-1.

1 INTRODUCTION

Scorpius X-1 (Sco X-1) was the first extra-solar X-ray source to be discovered (Giacconi et al. 1962) and remains a challenging object to explain after over 50 years of study. It is a low-mass X-ray binary (LMXB) and the prototype of the subclass of Z sources, so-named after the locus of points in an X-ray colour–colour diagram (Fig. 1; Hasinger & van der Klis 1989). Z sources are generally believed to be accreting at high rates, near or above the Eddington limit, as compared to the more numerous atoll sources which accrete at lower rates. They are subdivided into Sco-like systems, behaving like Sco X-1 and Cyg-like systems similar to Cyg X-2. Various attempts have been made to associate these different classes and subclasses of neutron star LMXB with other distinctive characteristics, for example the neutron star magnetic field or our viewing angle, but these are difficult to reconcile with the behaviour of the transient LMXB XTE J1701–462 which was observed to move from Cyg-like Z source to Sco-like Z source to atoll source during the decay of its outburst (Lin, Remillard & Homan 2009; Homan et al. 2010). This suggests that the primary distinguishing feature between the atoll class and the two Z subclasses is simply the accretion rate.

The three branches of the Z-diagram are the horizontal branch (HB), the normal branch (NB), and the flaring branch (FB), with Sco X-1 spending most of its time on the NB and FB. The HB–NB transition is referred to as the hard apex and the NB–FB transition is the soft apex. The Z-diagram is often assumed to be a monotonically increasing sequence in mass accretion rate from HB to FB (e.g. Psaltis, Lamb & Miller 1995), but this is challenged by some models with Church et al. (2012) arguing that the lowest mass transfer rate occurs at the soft apex, with both the NB and the FB representing different modes of increasing accretion, while Lin, Remillard & Homan (2010) infer no change in mass transfer rate at all around the diagram. There is currently no widely accepted consensus on the correct interpretation of the Z-diagram.

The optical counterpart to Sco X-1, V818 Sco, was discovered by Sandage et al. (1966), opening the door for subsequent multi-wavelength studies aiming to study optical variability and relate X-ray and optical behaviour (Hiltner & Mook 1967, 1970; Bradt et al. 1975; Canizares et al. 1975; Mook et al. 1975). This early work established large amplitude optical variability, with several preferred optical flux levels resulting in bimodal or trimodal flux

★E-mail: rih@phys.lsu.edu

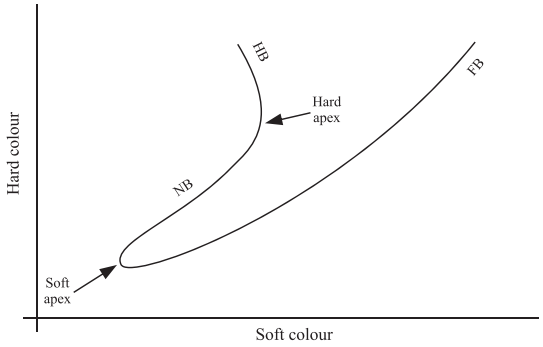

Figure 1. Schematic Z-diagram for Sco X-1 based on Hasinger & van der Klis (1989). The three branches are annotated HB (horizontal branch), NB (normal branch) and FB (flaring branch). Note that the HB is short, and nearly vertical in Sco-like Z sources.

histograms. At fainter optical levels, optical variations appeared uncorrelated with X-rays, or at times anti-correlated, but when the source was brightest a correlation emerged with the large X-ray variations in the FB. Subsequent similar studies (e.g. Augusteijn et al. 1992; McNamara et al. 2003) have confirmed these patterns with better data.

The discovery of optical and X-ray correlations at some times also raises the possibility of using simultaneous rapid data to measure lags between the X-ray and optical on the assumption that optical variability is produced by thermal reprocessing of incident X-rays by the disc and companion star. Lags of the order of seconds are expected due to light travel times within the binary and can be used to identify where light is being reprocessed and possibly even measure system parameters (O'Brien et al. 2002). The first thorough studies were by Ilovaisky et al. (1980) and Petro et al. (1981). Both groups found that the optical was correlated, and lagged behind the X-rays with some smearing of the reprocessed variability. Petro et al. (1981) found that time-scales less than about 20 s were smoothed out. McGowan et al. (2003) performed a more sophisticated analysis of these data sets, but found that in some cases the optical could not be straightforwardly described with a simple reprocessing model. Where this method did work, they found a lag of 8.0 ± 0.8 s and smearing of 8.6 ± 1.3 s. Muñoz-Darias et al. (2007) performed a modern study using fast CCDs and narrow-band filters simultaneously with the *Rossi X-ray Timing Explorer*. They found lags of 11–16 s associated with the Bowen blend emission lines around 4640 Å at the top of the FB, and attributed these to reprocessing on the companion star. Correlations were also found at the bottom of the FB with lags of 5–10 s, which were attributed to reprocessing in the disc. Britt (2013) performed an extensive study spanning all orbital phases and a range of states, and found that correlations were only present when Sco X-1 was in the FB. No orbital modulation was seen in the lags, suggesting the reprocessed signal was dominated by the disc, at least in the continuum.

The binary period was identified as 18.9 h based on the discovery of a photometric modulation by Gottlieb, Wright & Liller (1975) in archival photographic plates and spectroscopically confirmed by Cowley & Crampton (1975). Because of the large amplitude aperiodic variability in the source, the orbital modulation cannot be seen in individual light curves and only emerges when large data sets are folded (Gottlieb et al. 1975; Augusteijn et al. 1992; Hynes & Britt 2012). The photometric modulation arises from X-ray heating of the inner face of the donor star and takes the form of a sinusoidal modulation of full amplitude 0.13–0.26 mag. Augusteijn et al. (1992) found that the amplitude and phasing of modulation was the same in both high and low states, but no data set has been sufficiently comprehensive to permit detailed study of the light-curve morphology. Irradiation of the donor star also produces narrow emission lines of N III and C III (the 4640 Å Bowen blend noted above) phased as expected based on the photometric modulation (Steeghs & Casares 2002). These provide the potential to determine the system parameters, although since they do not trace the motion of the centre of mass, and we remain uncertain about the binary mass ratio and inclination, there are substantial uncertainties. The most comprehensive analysis has been performed by Mata Sánchez et al. (2015) who conclude that the neutron star must have a mass less than 1.73 $M_\odot$ at 90 per cent confidence.

A key ingredient in interpreting observations of any LMXB is the binary inclination. In Sco X-1, this is generally taken to be low. Fomalont, Geldzahler & Bradshaw (2001) estimated $i = 44^\circ \pm 6^\circ$ from modelling of the orientation of the twin radio jets. This method does not in general give a reliable measure of the orbital inclination as the jets may be misaligned with the accretion disc. For example, in two microquasars there is a clear discrepancy between inclinations derived from jets and those from optical data (Maccarone 2002) and in SS433 we observe precession of the radio jets on a 164 d period attributed to misalignment between the jet and the orbital axis (Hjellming & Johnston 1981). On the other hand, in Sco X-1 Fomalont et al. (2001) find the jet inclination to be stable over five years, implying negligible precession and a jet aligned with the orbital plane, suggesting that this measurement may be reliable. Mata Sánchez et al. (2015) independently examine system parameters derived from optical spectroscopy and conclude that an inclination higher than 40° would require a neutron star of mass below 1.4 $M_\odot$.

Beginning in 2009 May, the *Kepler* mission monitored a fixed area of the sky to search for extra-solar planets (Koch et al. 2010). With the failure of a second reaction wheel in 2013 May, the primary mission came to an end as precise pointing could no longer be maintained. *Kepler* received a second wind in the form of the K2 mission (Howell et al. 2014). Pointing could be maintained with the aid of the solar wind provided the satellite only pointed at targets on the ecliptic, and so the K2 mission has taken the form of a series of three month campaigns spaced around the ecliptic. Campaign 2 was observed from 2014 August 23 to November 13, and fortuitously included Sco X-1 in the field. We report here our analysis of this data set in conjunction with simultaneous X-ray monitoring with the *Fermi* GBM and MAXI. Scaringi et al. (2015) and Hakala et al. (2015) report independent analyses using *Kepler* and MAXI only. In Section 2 we describe the data sets used. We analyse the orbital modulation in Section 3, allowing us to remove its effects and examine the residual variability in Section 4. Section 5.3 examines the statistical properties of individual flares identified when the source is brightest. We proceed to incorporate X-ray data into the analysis in the form of X-ray/optical flux–flux diagrams in Section 6 and then examine lags in Section 7. Finally, in Section 8 we use states identified in *Kepler* data to sort GBM and MAXI data by spectral state and hence construct average spectra for each state. We round up by discussing some interpretations of our results in Section 9, propose a possible mechanism for relating the X-ray and optical behaviour in Section 10, and finally summarize our findings and conclusions in Section 11.

2 OBSERVATIONS

2.1 *Kepler*

Kepler observed Sco X-1 in short-cadence mode, with 54.2 s integrations, from Julian dates (JD) 245 6893.275 (2014 August 23) to

245 6972.058 (2014 November 10), for a total of close to 78.8 d, with few gaps in a relentless cadence. These *Kepler* observations, as part of the K2 mission, were proposed, accepted, and observed for us under K2 proposal GO2026 (R. Hynes principal investigator) and independently by other teams. The images were sent to the ground with a small 'postage stamp' of 14 by 12 pixels (with seven pixels in the corners missing). Each pixel is 4 arcsec^2, with the detector resolution being somewhat smaller, so the star images are undersampled. Sco X-1 is the only star in the field. The entire *Kepler* experience is that the stability of the 'absolute' photometry is much better than the parts-per thousand level. The photometric aperture chosen was a 41 pixel area that covered effectively all the Sco X-1 light, with this aperture being sufficiently large so that the usual small movements of the *Kepler* spacecraft made for no flux shifting in-and-out of the aperture. Since *Kepler* data are flat-fielded with a pre-launch flat, there potentially are variations introduced by motion of the source with respect to secular changes in the flat-field. These are seen in other K2 targets, but are below 1 per cent and negligible compared to the intrinsic source variability. The typical source flux is around 140 000 e^- s^{-1}, so the Poisson one-sigma uncertainty is around the 0.04 per cent level per integration. This photometric uncertainty is also negligibly small compared to the unresolved rapid variations of Sco X-1. Except where artefacts noted below occur, we then expect *all* the variability seen to be intrinsic to Sco X-1 itself. Further evidence for this is the absence of a white noise component even at the highest frequencies in the power spectra shown by Scaringi et al. (2015).

The flux of Sco X-1 was extracted from the images with the usual *Kepler* pipeline. The output has the flux inside our 41-pixel photometry aperture, with a background subtraction from the rest of the image, all reported in e^- s^{-1}. The wavelength sensitivity is that of the *Kepler* CCD with no filters, resulting in a so-called '*Kepler* magnitude' that covers a broad-band over the usual *B*, *V* and *R* range. There is no easy or accurate means to convert from the *Kepler* magnitude to any standard magnitude for an object such as Sco X-1 with a non-stellar spectral energy distribution. Some variation in apparent brightness might be introduced by changes in spectral shape for such a broad filter. Augusteijn et al. (1992) found a difference of 0.024 ± 0.005 in the $(B - V)$ colour of Sco X-1 between optically bright and faint states. Since this corresponds to only about a 2 per cent variation in F_V/F_B, we expect colour changes to make a negligible contribution to the variations we observe.

The *Kepler* light curves are generated with time stamps for the middle of the exposure expressed as a barycentric Julian date (BJD) in the barycentric dynamical time (TDB) system. Hereafter we will follow Eastman, Siverd & Gaudi (2010) and refer to such dates in the format $\mathrm{BJD_{TDB}}$. Throughout this work, we will use this notation to indicate both the date convention and time system used for original data products and those we actually combine and analyse. Neglecting the time system results in errors of the order of a minute which is not negligible compared to the *Kepler* exposure times. A thorough discussion of the importance of specifying time systems and definitions of the systems used in this paper is provided by Eastman et al. (2010).

We know of three data artefacts that can affect our light curve. First, images can have discrepant fluxes during occasional reaction wheel angular momentum desaturation events due to the movement of the Sco X-1 image. Fortunately, all such instances are flagged in the *Kepler* pipeline output. All fluxes taken during times of desaturation events have been deleted from our data set together with periods of coarse pointing around them. In addition, time bins following a desaturation event occasionally display clearly discrepant fluxes, even when not flagged, and these have also been systematically deleted. In all, we discarded 1956 data points. Secondly, in the usual way, cosmic rays occasionally hit within a photometric aperture, leaving apparent extra flux. In other *Kepler* data sets, we see that this happens in a given aperture on the order of a few times per day, with detected events ranging from 20 to 400 counts. This is completely negligible in our Sco X-1 light curve. Thirdly, during the time period $\mathrm{BJD_{TDB}}$ 2456 911.23 to 2456 912.05, solar flares made for some extra flux in the photometry aperture. Our experience with *Kepler* point sources with no fast variability shows that the effects are random enhancements of up to 1000 counts for some time bins during this interval. Such excess is negligibly small compared to the fast variability in the base flux from Sco X-1, so we have not excised any light-curve points during this time interval of solar activity. In all, we have 115 680 fluxes, all tied to an accurate $\mathrm{BJD_{TDB}}$, to form our *Kepler* light curve, with typically better than one per cent photometric accuracy.

The *Kepler* light curve creates some difficulties in estimating uncertainties. Because of the exquisite data quality, instrumental errors are negligible compared to the intrinsic variability in the source. This means that the noise characteristics are those of the source, not of white noise. In places, the light curve is dominated by short flares of increasing flux (only), so the local flux distribution is asymmetric and distinctly non-Gaussian. In other places, there is little very short time-scale variability. Furthermore, the intrinsic time-scale of the variability introduces an auto-correlation into the data. The result is that the uncertainties on the data points are not independently and identically distributed, and are non-Gaussian. This invalidates many usual statistical methods (e.g. χ^2 fitting). A more robust approach that uses the distribution within the data set itself is the bootstrap (Efron 1979), where data points are randomly drawn from the light curve, with replacement, to create many resampled versions of the light curve, which are then analysed identically to the data. In this case, we require a bivariate bootstrap where we resample (time, rate) pairs, as we need to preserve the timing information if we are to analyse periodic modulations or correlations with other wavebands.

The simple bootstrap method is known to significantly underestimate uncertainties when the data are autocorrelated. In this case, the most commonly used modification is the block bootstrap (Künsch 1989; Liu & Singh 1992). In this case, rather than resampling individual points, we resample blocks of consecutive points with the length of block chosen to preserve the autocorrelation characteristics of the data. There are a variety of specific implementations of this idea. For this work we adopt the stationary bootstrap of Politis & Romano (1994) which uses a geometric distribution of block lengths and wraps around from the end of the time series back to the beginning. After testing this method on simulated data sets with the same sampling, sinusoidal modulation, and noise power-spectrum to Sco X-1, we adopted an average block length of 2880 points, corresponding to about 2 d. This is longer than the orbital period and the typical time-scales of variability and in simulations recovers correct uncertainties.

2.2 *Fermi* GBM

The Gamma-ray Burst Monitor (GBM) is one of the two instruments on board the *Fermi Gamma-Ray Space Telescope*. It consists of 14 detectors: 12 Na I detectors and two BGO detectors. Typically, three to four Na I detectors view an Earth occultation within 60° of the detector normal vector. The two BGO detectors are located on opposite sides of the spacecraft and view a large part of the sky in the energy range 150 keV to 40 MeV. None of the GBM

detectors has direct imaging capability. GBM has two continuous data types: CTIME data with nominal 0.256 s time resolution and eight-channel spectral resolution, and CSPEC data with nominal 4.096 s time resolution and 128-channel spectral resolution. The results presented in this paper use the lower spectral resolution CTIME data and the higher spectral resolution CSPEC data from the Na I detectors for the light curves and spectral studies, respectively.

Fermi was launched in 2008 June into a 25.°6 inclination orbit at an altitude of 555 km. The diameter of the Earth as seen from *Fermi* is 135°, so roughly 30 per cent of the sky is occulted by the Earth at any one time. One complete orbit of the spacecraft allows over 85 per cent of the sky to be observed. The Earth Occultation Technique (Wilson-Hodge et al. 2012) allows GBM to monitor the fluxes of known point sources. The technique involves fitting a model consisting of a quadratic background plus source terms to a short 4 min window of data centred on the occultation time of the source of interest. The precession of the orbital plane allows the entire sky to be occulted every 26 d (half the precession period for the *Fermi* orbit), though the exposure is not uniform. All GBM data for Sco X-1 coinciding with the *Kepler* observations were analysed. In order to maintain data quality, we apply several event selection cuts, for instance eliminating occultations with high satellite spin rate and data from South Atlantic Anomaly crossings. Other cuts were applied to remove occultations that coincide with solar flares. The times of the solar flares are determined by the *GOES* satellite.

The original occultation light curve had time stamps for the middle of the occultation in mission time. We have corrected this to terrestrial time (TT) heliocentric Julian dates ($\mathrm{HJD_{TT}}$), which are within four seconds of the $\mathrm{BJD_{TDB}}$ used for the *Kepler* light curve (Eastman et al. 2010). Our observations extend over a 78.8 d interval, so a correction to the heliocenter or the barycenter is required for phasing our observations correctly, and for relating them to a known ephemeris, but the difference between $\mathrm{BJD_{TDB}}$ and $\mathrm{HJD_{TT}}$ is negligible compared to the *Kepler* exposure time.

2.3 MAXI

We also used X-ray monitoring data from the Gas Slit Camera (GSC) of the Monitor of All Sky Image (Matsuoka et al. 2009, MAXI) on the *International Space Station (ISS)*. The GSC has a $160^\circ \times 1.^\circ5$ slit camera mounted at a fixed orientation pointing away from the Earth. Targets are usually detected once per 92 min *ISS* orbit. Transit times across the slit are 45–120 s, so source fluxes are originally obtained with a comparable timing precision to *Kepler*. Since public light curves are reported in observation period times we instead obtained scan times from the *MAXI* team (T. Mihara, 2015, private communication) corresponding to the time during slit transit of maximum transmission (i.e. effective mid-exposure). These times are reported in coordinated universal time modified Julian dates ($\mathrm{MJD_{UTC}}$), where MJD = JD − 2400 000.5. We have converted $\mathrm{MJD_{UTC}}$ to $\mathrm{HJD_{TT}}$, consistent with our *Fermi* light curves and within four seconds of the $\mathrm{BJD_{TDB}}$ used with the *Kepler* light curve. This should result in tighter correlations between X-ray and optical flux and sharper cross-correlation functions (CCF) than earlier works using public data products. The GSC has a nominal energy range of 2–30 keV. The standard bandpasses which we used are defined as 2–4 keV, 4–10 keV, and 10–20 keV, as well as a combined 2–20 keV band.

3 ORBITAL MODULATION

We expect to find an orbital modulation of amplitude ∼0.1 mag in the *Kepler* data as seen in previous studies described in Section 1. Fitting a sine wave to the data we measure a photometric period of $P = 0.787\,47(72)$ d, where the uncertainty is estimated by bootstrap resampling as described in Section 2.1. This is comparable to other estimates obtained from archival photometry (Gottlieb et al. 1975; Hynes & Britt 2012; Galloway et al. 2014), and consistent within errors with the most precise spectroscopic period of $P_{\mathrm{orb}} = 0.787\,311\,4(5)$ d measured using Bowen emission lines (Galloway et al. 2014). For the remainder of this work we will adopt the latter period.

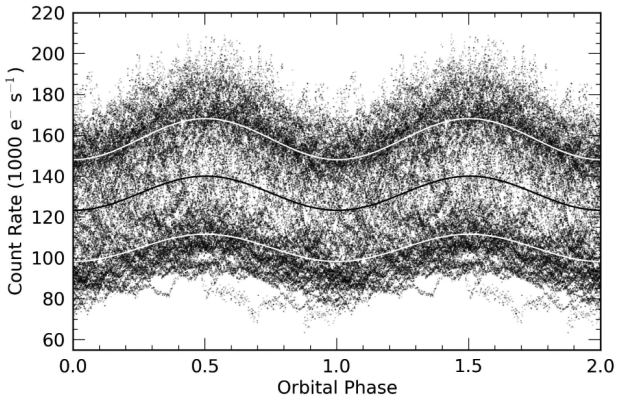

Figure 2. *Kepler* data folded on the orbital period of Galloway et al. (2014). The solid black line is a sinusoidal fit to the raw data. Solid white lines are the same fit scaled to match the two dominant groups of points. Note the distinct bimodal behaviour in optical brightness, which we are calling high and low states and also that both states apparently share the same modulation.

In Fig. 2 we show the *Kepler* data folded on Galloway's period. We also show a sinusoidal fit to the full data set. The sine wave appears to describe the modulation fairly accurately; we will discuss possible deviations from a pure sine wave shortly. The phase-offset with respect to the T_0 defined by Galloway et al. (2014) is only 0.007 and the full amplitude is 0.14 mag, comparable to earlier observations. We derive an updated time of photometric minimum as $T_0 = 2456\,932.7386 \pm 0.0016$ ($\mathrm{BJD_{TDB}}$) with the error estimated by bootstrap resampling. For comparison, the ephemeris of Galloway et al. (2014) predicts a time of minimum of $T_0 = 2456\,932.7430 \pm 0.0019$ ($\mathrm{HJD_{UTC}}$). Accounting for the difference between time systems this is a difference of 0.0052 d, or 0.007 in phase, as noted above. Combining the errors on the two measures, this is a 2.1σ difference. We conclude that the spectroscopic and photometric phases are coincident to a high precision, better than 1 per cent of an orbit. The difference does not have high statistical significance.

It can be clearly seen in Fig. 2 that the data follow a bimodal distribution, as noted by Scaringi et al. (2015) and Hakala et al. (2015), and comparable to what was found by earlier studies. As shown in Fig. 2, the fitted mean modulation appears to separate the high- and low-state data quite well. We could use this dividing line to separate the data into high- and low-state samples more cleanly than was possible ignoring the modulation. In practice, the mean flux, as used by Hakala et al. (2015), or the mean modulation, as shown in Fig. 2, has the undesirable property that the adopted division between states depends on the relative time spent in each state, so we adopt a somewhat different procedure. We instead detrend the light curve by dividing by a sine wave with the same fractional amplitude but unit mean $[1 - A\cos(2\pi\phi)$, where A is the fractional half-amplitude and ϕ is the orbital phase], and then define the state boundary at 140 000 $\mathrm{e^{-1}\ s^{-1}}$ after detrending. The choice of the latter is motivated by examination of the optical versus X-ray

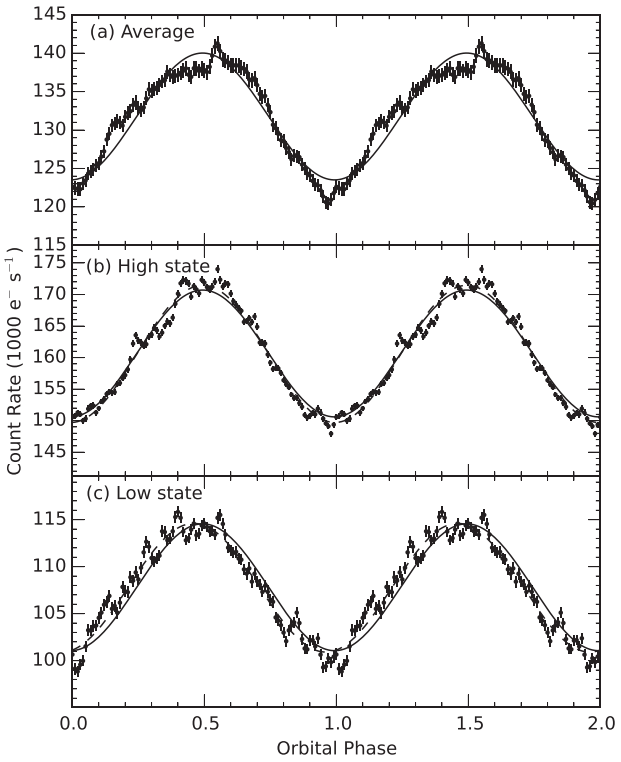

Figure 3. Phase-binned data compared to sinusoidal fits. Solid lines are the fit to the full data set, rescaled to match the mean flux in each panel. The dashed lines in panels (b) and (c) are fits to the data in those panels only. Note that the dashed lines are very close to the solid line and indistinguishable in some places and that the apparent deviations from a sine wave are not statistically significant.

relations in Section 6 and we will defer more detailed discussion until that point. With this prescription, the state classification of a given point is independent of the relative time spent in each state. Throughout this work we will refer to the two optical states as the high state and low state, and this terminology should not be confused with the high and low states of black hole LMXBs (also known as thermal dominant and hard states, respectively). These are not used in discussing Z sources, so there should be no confusion in this work.

We show in Fig. 3a comparison of phase-binned light curves, both the average of all the data and separate averages of high- and low-state data, along with the sinusoidal fit to the whole unbinned data set and fits to the individual binned samples. A sinusoidal fit is to be expected for a low inclination view of a heated donor; the light curve becomes progressively non-sinusoidal at higher inclinations, but at low inclinations ($\lesssim 50^\circ$) it is almost indistinguishable from a sine wave. We see that all the curves are quite close to sinusoidal, as expected given the inclination estimates (see Section 1), and that deviations are comparable to the amplitude of residual variability that has not averaged out.

There is no clear difference in amplitude between high and low states. Formally, we measure a full amplitude of 0.147 ± 0.012 mag in the low state and 0.151 ± 0.008 mag in the high state. The low state does suggest a small shift to earlier phases. We measure the phase offset between high and low state to be 0.032 ± 0.024, with the low-state data leading the high state. If real, this might suggest either changes in the light distribution on the secondary star, or changes in disc asymmetry between the states. It is not significant at the 2σ level, however, and so may be an artefact of the random realization of aperiodic variability.

Examining the folded light curves, there appear to be apparent deviations from a sinusoidal light curve in the average light curve, and in particular it is noticeably more V-shaped at minimum than a pure sine wave. This is reminiscent of a grazing partial eclipse of the accretion disc, contrary to all the evidence for a low inclination (Section 1). We note, however, that the amplitude of fluctuations is comparable at other phases (e.g. near maximum). We also tried folding subsets of the data taking either the first and second 40 d period, or alternating odd and even two-day segments. In neither case was the effect seen in both subsets of the data, and these subsets show quite large deviations due to variability that has not averaged out. The eclipse-like feature, and indeed all the deviations from a sinusoidal form, appears therefore to be coincidental and not significant. In summary, we find no significant deviations from a sinusoidal modulation, and no compelling differences in phase or amplitude of the modulation between the low and high states. We note that this conclusion is a little different to that drawn by Hakala et al. (2015). While they conclude that the amplitude is lower in the low state, they express it relative to the mean overall flux, rather than the mean low-state flux. The folded light curves they show do show approximately constant *fractional* amplitude when compared to the mean flux of each state and this is consistent with our finding of equal amplitudes in magnitude. Hakala et al. (2015) also suggest that there are changes in morphology between states. As argued above, we believe that these are non-repeatable artefacts caused by not sufficiently averaging out variability. Since our state division is defined differently to theirs, our folded light curves will not average over variability in the same way, and so would be expected to look somewhat different. Hakala et al. (2015) used a fixed rather than phase-dependent division between states. This will mistakenly assign low state data to the high state at phase 0.5 and vice versa at phase 0.0. This may have the effect of distorting their state-dependent light curves leading to an underestimate of the derived modulation amplitudes.

We can also examine the standard deviation of the folded light curves for the high and low states. We show this in Fig. 4, with a coarser binning than used for the mean light curve due to the lower signal-to-noise ratio in the standard deviations than in the mean light. Surprisingly, the variability does appear to have a different phase dependence in the two states, even though the mean light does not. We find that in the high state the variability is modulated in the same way as the mean light, whereas in the low state we see little if any modulation. Put another way, in the low-state non-orbital variability has a constant absolute standard deviation (in flux), whereas in the high state it has a constant fractional standard deviation. To investigate the significance of this result we repeated the analysis using bootstrap resampling as done earlier in this section. We quantify the modulation by fitting a sine wave of fixed period and phased the same as the mean modulation, leaving the amplitude and zero-point as free parameters. We find from 1000 samples that the modulation amplitude in the high state is 7.0 ± 3.6 per cent, while in the low state it is -0.4 ± 3.4 per cent. This leaves the difference in behaviour suggestive but inconclusive.

If the difference in modulation of the variability between the normal and FB is real, it suggests that in the high state, the variability is imprinted on all of the emission by a common source. Since the high state appears to be associated with the X-ray FB where short-term X-ray-optical correlations are seen (Muñoz-Darias et al. 2007; Britt 2013; Scaringi et al. 2015, Sections 4 and 6), the likely mechanism is reprocessing by both the disc and secondary star of

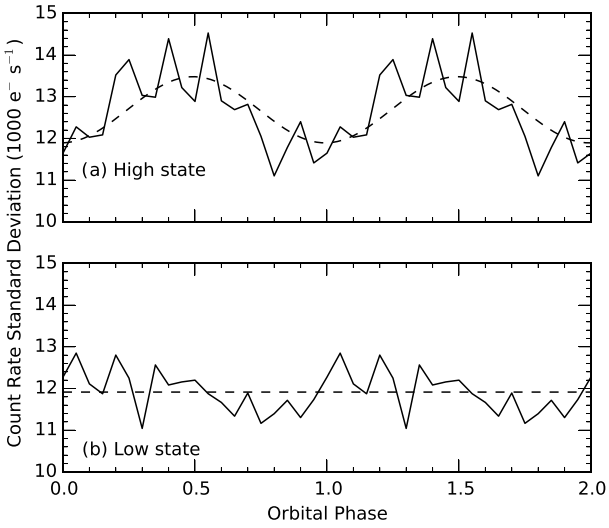

Figure 4. Standard deviations within phase-binned *Kepler* data as a function of orbital phase and state. During the low state, the variability is essentially constant throughout the orbit, whereas during the high state, Sco X-1 is more variable around phase 0.5 (when the companion star is viewed behind the neutron star).

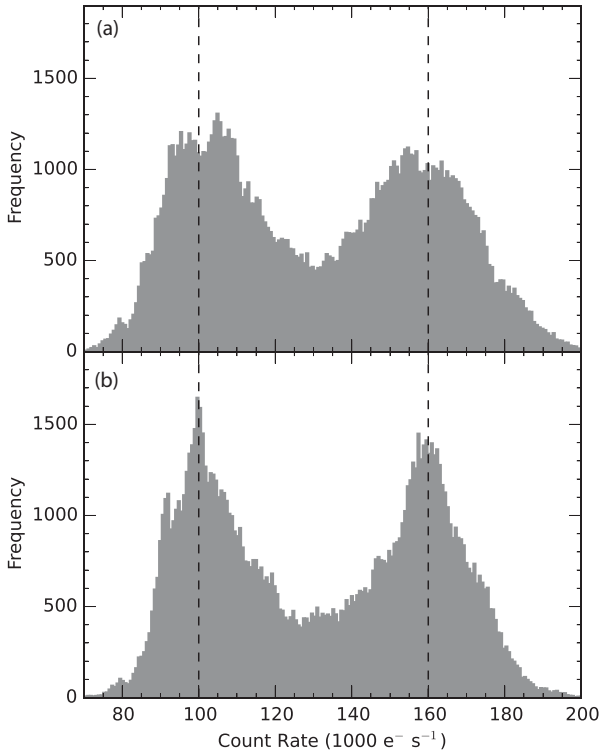

Figure 6. Flux histograms before (a) and after (b) removing the orbital modulation. Dotted lines are placed at 100 000 e^- s^{-1} and 160 000 e^- s^{-1} to mark the two main peaks. The histogram clearly shows that Sco X-1 is usually in either a fairly narrow high state or low state, with the fill in the middle caused by transitions (or failed transitions) between the two states.

X-ray variations. In the low state, the mean light curve indicates that irradiation of the companion is still occurring, but the aperiodic variability appears to be dominated by the disc, since it does not modulate strongly on the orbital period. This is consistent with the lack of clear, positive X-ray-optical correlations in the NB which appears to correspond to the low state (Britt 2013; Scaringi et al. 2015, Sections 4 and 6).

4 DETRENDED LIGHT CURVES

In Section 3 we fitted the sinusoidal orbital modulation and produced a prescription for detrending the light curve. This can be expected to produce simpler light curves, and also cleaner division into states in flux histograms. We show the whole detrended light curve in Fig. 5. The bimodal distribution is clear even here, with irregularly alternating high and low states and superposed faster variability. The low state shows mostly brightening episodes, while the high state shows both fast flares and slower dips. We will reserve the term 'flares' to refer to the discrete, fast variations in the high state (which corresponds to the X-ray FB as noted above), and refer to the slower variations as brightenings or dips. The latter resemble incomplete or failed state transitions.

We show histograms before and after detrending the orbital modulation in Fig. 6. The improvement is pronounced near the peaks, but some overlap between the states remains. This is to be expected,

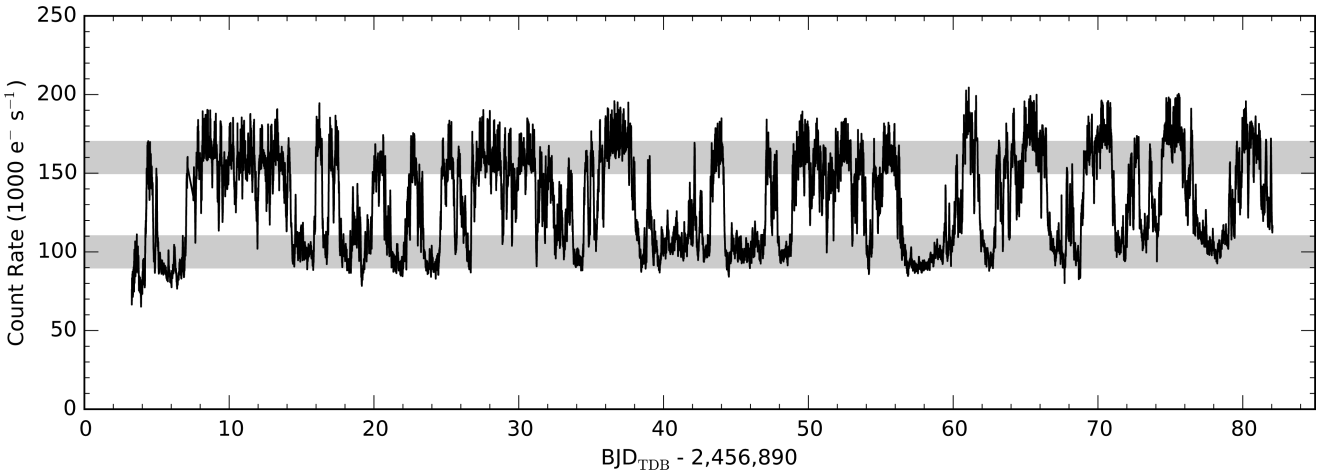

Figure 5. The whole *Kepler* light curve after removing the orbital modulations. Upper and lower bands correspond to fluxes around the two peaks of the histogram in Fig. 6. This is the first optical light curve to show the structure of the transitions between high and low states, with characteristic times in each state lasting for typically two to five days.

as state transitions are well resolved, and intrinsic variability within the states may also result in some overlap.

A single long observation such as provided by *Kepler* is ideal for putting historical studies of flux histograms into context. These studies showed a variety of bimodal and trimodal histograms, with variations from year to year. These can be interpreted in two ways; either there are three distinct optical states, of which sometimes only two are seen, or there are only two states which change in brightness enough that incompletely sampled data might show them appearing as three states. In Fig. 7 we show the histograms of the *Kepler* data subdivided into 10 consecutive segments each of about eight days duration, long enough to sample a range of states. We do see variations in the flux level of the high and low states, and the separation of the two states also clearly varies. At no point do we see a clear trimodal distribution. However, the variations we see over the course of about three months are not large. The lowest peak of the low state corresponds to about 0.15 mag below its average value and the highest peak of the high state is about 0.1 mag above the mean. Historical histograms sometimes show trimodal distributions with peak separations ∼0.5 mag within a single month. This could not be reproduced by any reasonable sampling of the *Kepler* data. This analysis then requires that the historical behaviour be different to that seen during the *Kepler* observation. Either the flux levels of the states were more variable, or a third state not seen by *Kepler* was present. Since only the NB and FB can be clearly identified in the MAXI Z-diagram (Section 6) and these can be associated with *Kepler* low and high states, it is possible that the missing third state is associated with the HB (cf. Vrtilek et al. 1991). The subdivided histograms also show that the infilling between the peaks in Fig. 6 may be largely a consequence of the movement of the peaks. Fig. 7(a), for example, shows negligible infilling between the peaks and may provide the best indication of the intrinsic flux distributions of the two states. Both peaks show asymmetry of character similar to that suggested by Scaringi et al. (2015), with the high state showing a low tail and the low state showing a high tail. These asymmetries presumably arise from the intrinsic asymmetry of the failed transitions (brightenings in the low state and dips in the high state.)

Scaringi et al. (2015) used MAXI colours to identify FB and NB epochs. They found that the high state was usually associated with the FB and that the low state corresponded to the NB. They also found that the optical flux was a better predictor of X-ray branch than X-ray fluxes alone. Since we cannot classify states based on colour with GBM data, for this work we will use the optical fluxes to divide data into high states and low state using a dividing line at 140 000 e^{-} s^{-1} (Section 6). These provide a proxy for the X-ray FB and NB, but we should not assume that they are completely synonymous. We will examine the association between optical and X-ray states more carefully in Section 6.

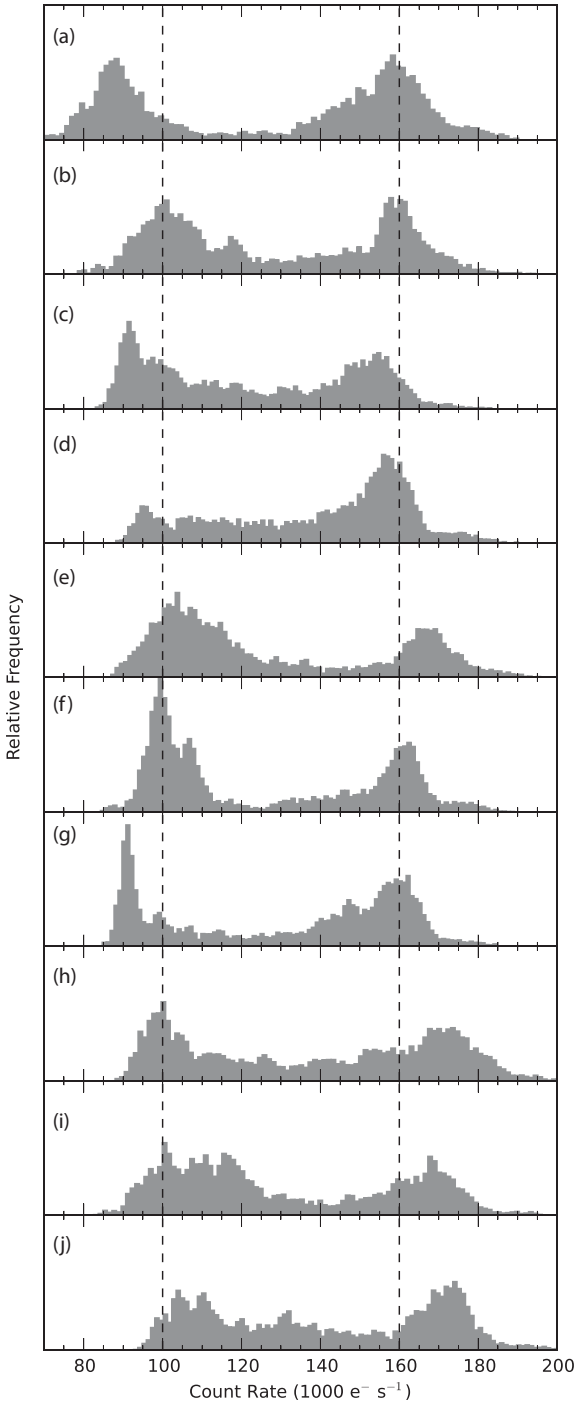

Figure 7. Histograms of 10 equal subsets of the light curve after removing the orbital modulation. Dotted lines are as indicated in Fig. 6. For all the *Kepler* data, Sco X-1 only shows two states, with these moving around somewhat in brightness.

5 DISCRETE STATISTICAL ANALYSES

5.1 High-state durations

The *Kepler* light curve represents an unprecedented source of information on the statistical distribution of source states which is relatively free of completeness effects since it contains very few gaps. We have so far considered distributions of continuously variable fluxes. We now move to consider discrete states, transitions, and events. We begin by considering typical durations of the high states. We note that definition of high states is relatively straightforward, since they are characterized by a quite flat plateau with signature flares. An analogous distribution of low states would not be possible, as the low state merges seamlessly into transitions.

We define a continuous high state as a period when the source showed a relatively flat plateau which included flares. A continuous high state is terminated by any clear dips below the plateau level. In some cases, e.g. around days 7–14 in Fig. 5, this breaks a relatively long high state into multiple shorter episodes. We believe this is an appropriate definition, as the high state is interrupted by an attempt, albeit a failed one, to transition to the low state. With this definition

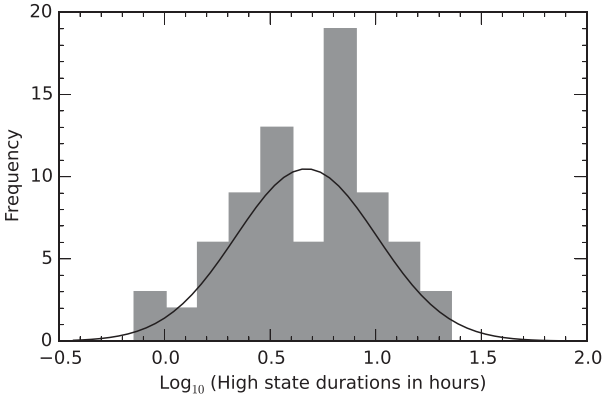

Figure 8. Distribution of durations of uninterrupted high-state episodes. The fit is a log-normal distribution described in the text.

we identify 77 high-state periods of durations 0.7–22.8 h. There is a clear preference for quite short durations, with longer uninterrupted periods becoming increasingly improbable. The distribution can be fit by a log-normal distribution with shape parameter 0.77 and scale parameter 4.7 h. That is to say, the logarithms of high-state durations follow a Gaussian distribution with standard deviation (of the logarithms) of 0.77 and median duration 4.7 h. The fit is acceptable to a Kolmogorov–Smirnov test with a p-value of 0.45. We show the resulting distribution of durations together with the fitted distribution in Fig. 8. A log-normal distribution arises when results are a product of multiplication of a series of independent processes. Such a model for X-ray binary variability is indeed now favoured in the form of the propagating perturbation model in which local mass transfer fluctuations at progressively smaller radii imprint their signature multiplicatively on the overall mass transfer rate and hence source brightness (Lyubarskii 1997). This does appear to lead to a log-normal distribution of fluxes (Uttley, McHardy & Vaughan 2005; Gandhi 2009). If our high states reflect the length of time where the flux exceeds a threshold level, then their duration distribution would be related to the flux distribution, and so a log-normal duration distribution might naturally be expected.

We can also take a broader definition of high states, as we see extended periods where the high state is preferred, even if brief partial or complete transitions back to the low state occur. The longest such episodes last for about a week, and are followed by an extended low or low/transition period. We will discuss the possible significance of this in Section 9.

5.2 Transition time-scales

It is quite striking that there is a similarity of time-scales among all transitions between the high and low states. This applies to full transitions, brightenings in the low states, and dips in the high states. In fact, if the source brightness is plotted on a magnitude scale, these transitions appear to be near-linear with a modest (but clear) range of gradients. This suggests an exponential behaviour that can be characterized by an e-folding time, defining a time-scale for the process mediating the optical transition.

We compile measurements of all such transitions where a near-monotonic rise or decline segment of at least 10 per cent in flux could be identified and show their distributions in Fig. 9. We find no convincing dependence of the transition time-scale on either the mean brightness or the amplitude of the transition, suggesting that large-state transitions, low-state brightenings, and high-state dips are all intimately connected. There does appear to be some

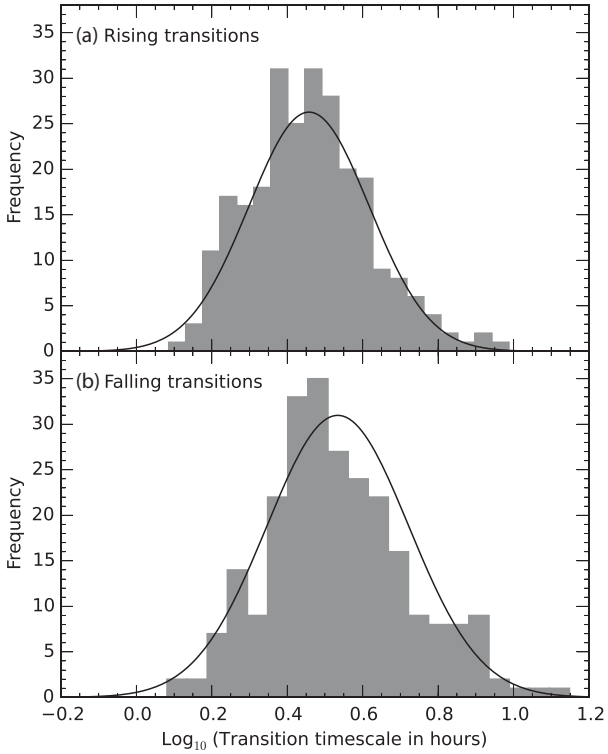

Figure 9. E-folding time-scales of transitions between high and low states, including failed transitions. The smooth lines are log-normal fits to the distributions described in the text.

difference between rise and decay time-scales, with slower decays more prevalent than slow rises, but the distributions of rise and decay time-scales are strongly overlapping. A Kolmogorov–Smirnov test rejects a common distribution for the two at a significance of 99.9 per cent. Both rise and decay time-scale distributions are consistent with log-normal distributions with shape parameters of 0.37 and 0.43 and scale parameters (median time-scales) of 2.9 h and 3.4 h respectively. The fits are both acceptable to Kolmogorov–Smirnov tests with p-values of 0.96 and 0.17, respectively. The time-scales quoted are e-folding time-scales, not actual transition times. The ratio of optical fluxes between typical high and low states is 1.6 (Fig. 6), so the characteristic times to execute a full rising and falling transition are 1.7 and 2.0 h, respectively.

5.3 High-state flare characteristics

While Sco X-1 is on the FB it shows strong X-ray flares. We show some examples of corresponding events seen in optical light in the high state in Fig. 10. Detailed prior studies with simultaneous X-ray and optical time series show that the optical light from flares is a slightly delayed and smeared version of the X-ray flares, pointing to the optical flare flux coming from X-rays reprocessed by both the disc and the companion star (see review in Section 1). Our *Kepler* programme for Sco X-1 now has by far the longest and most completely sampled optical light curve. This long and steady coverage allows for the demographics of the flares to be well-measured. Detailed examination of the full light curve shows that the optical flares are distinct events with a fast rise, a roughly symmetric light-curve shape, durations of 5–20 min, all with nearly the same amplitude, and *only* occurring when Sco X-1 is in its nearly flat high state.

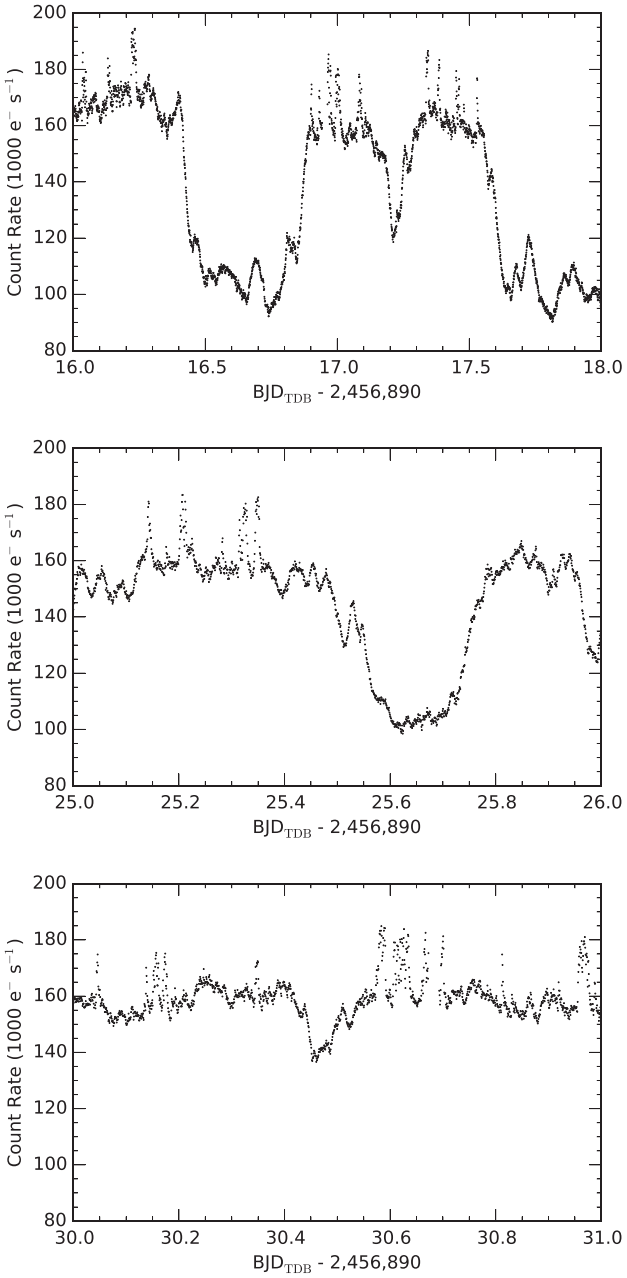

Figure 10. Examples of high-state *Kepler* light curves. When Sco X-1 is in its high state, it frequently displays fast flares, and these fast flares are only seen during the high state.

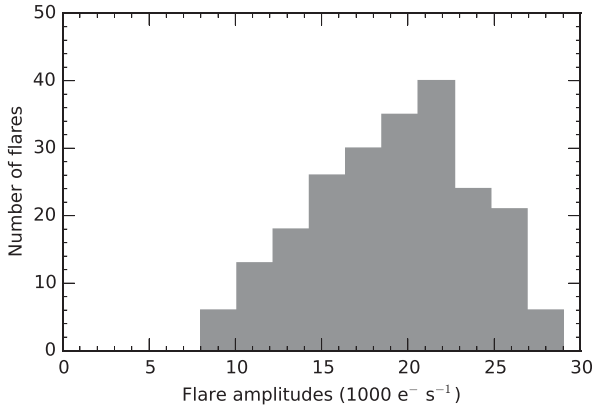

Figure 11. Distribution of high-state flare amplitudes. The amplitude of the fast high-state flares varies only over a fairly restricted range with a quite sharp upper cut-off.

The optical flares are distinct short-duration brightenings from the optical high state that always have a sudden start, a sharp peak, and a sudden stop. We see no case where there is any prolonged pre-flare or post-flare emission. To get some statistics on flare durations and rise/fall times, we have gone through the light curve and picked out by eye the bins that are the start, peak, and end of each optical flare. From these points, we can calculate the rise time, the fall time, the duration, and the amplitude of the peak of each flare. The histogram of the flare durations shows a peak at 9.4 min, with the central 67 per cent of the flares with durations between 8.3 and 16 min, and with the central 90 per cent of the flares between 5 and 31 min. If the longer duration flares are actually two or more flares superposed at nearly the same time which we could not resolve into separate flares, as appears to be the case, then the real upper limit for the duration of a single flare is roughly 20 min. Flares with significant flux and durations from 2 to 5 min would have been easily identified, so the deficit of <5 min duration flares appears to be real. Indeed, all the flares identified as having durations <5 min are tightly bounded by other flares such that the times tagged for the start and end are high above the usual floor. These short durations are therefore more like full-width-half-maximum durations, so the <5 min durations appear to be an artefact of flare bunching. There is no preference for rise times to be either faster or slower than fall times. So the optical flare light curves are distinct with steep rises, sharply isolated from the earlier and later variations, 5–20 min durations, and roughly symmetric shapes. We note that Scaringi et al. (2015) analysed the *Kepler* power spectrum in the high state and identified two structures, a red noise power law and a bump around 10^{-3} Hz, corresponding to time-scales of 15–20 min. This bump is presumably associated with the rapid flares which are distinct from the underlying flickering of the plateau level.

In looking at the light curve with Sco X-1 in its optical high state, it is apparent that all the optical flares have similar peak amplitudes above the non-flare level. This is apparent in the three panels of Fig. 10 and also in Fig. 16. To quantify this, we have constructed a histogram of flare amplitudes (see previous paragraph) from the peak level to the base level at the start or end of the flare. Our peak amplitude histogram (see Fig. 11) shows a peak around 20 000 e^- s^{-1}, with a minimum duration of 8000 e^- s^{-1} and a sharp upper limit of about 27 000 e^- s^{-1}. Our light-curve time resolution is 59 s, which is longer than the usual time at peak, so our peak fluxes will usually be underestimates by variable fractions, and this will lead to a moderate intrinsic scatter in the peak amplitudes. Another source of moderate intrinsic scatter for our measured amplitudes comes from partial overlaps for a small fraction of the flares, where the rise or decline of one flare adds to the peak flux of another flare, creating an apparently larger amplitude. The histogram shows sharp upper and lower limits on the flare amplitude. The upper limit is real and we can think of no artefacts or biases that would eliminate flares with amplitude >27 000 e^- s^{-1}. The real sharpness of the lower limit is problematic, because we cannot readily quantify the efficiency of our selection for low-amplitude flares. Looking at the light curves, we see few events that could be claimed to be flares with amplitude ∼8000 e^- s^{-1}, but we do see variations at the ∼2000 e^- s^{-1} level that might be low-amplitude fast optical flares. Thus we think that the optical fast flares do have a lower limit on their amplitude, but this conclusion is not of high confidence.

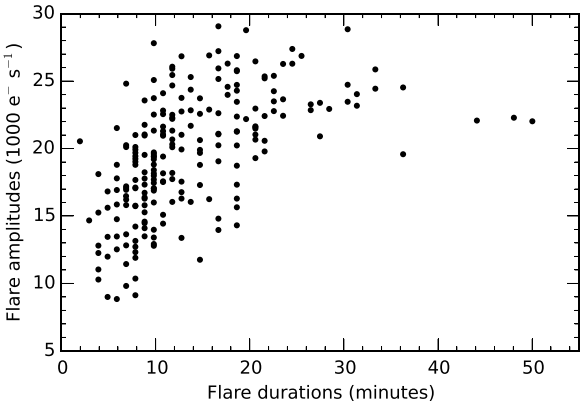

Figure 12. Relationship between durations and amplitudes of high-state flares. A significant and positive correlation shows that the larger amplitude flares have a strong tendency to be longer in duration. The flares with apparent duration longer than 30 min are likely just two or three flares spaced closely enough in time that we could not distinguish the individual flares.

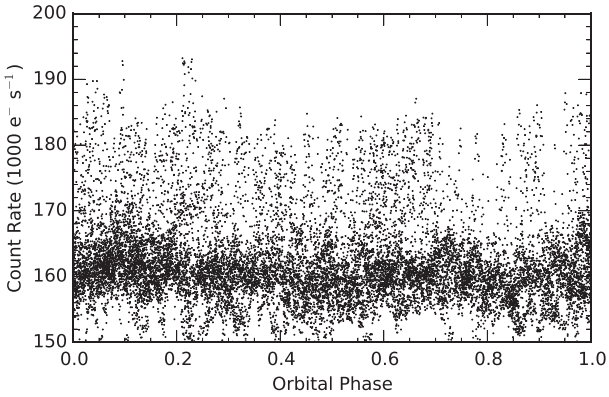

Figure 13. The first 30 d of *Kepler* high-state data folded on the orbital period. The orbital modulation has been corrected, slow variations in the baseline level have been subtracted out and excursions towards the low state have been excluded. This figure shows the upper limit on the flare amplitude (with flare maxima between roughly 185 000 and 192 000 $e^- s^{-1}$ above the baseline at 160 000 $e^- s^{-1}$). This figure also shows that the flare amplitude (scaled to take out the orbital modulation) and frequency do not vary with orbital phase.

From this analysis, it appears that the fast optical flares are all roughly of the same amplitude (∼20 000 $e^- s^{-1}$), and there is certainly a sharp upper limit on flare amplitude (∼27 000 $e^- s^{-1}$). An obvious interpretation is that the upper limit in the optical comes from a maximum luminosity associated with the nuclear burning event on the neutron star, much like in the case of X-ray bursters. This is consistent with the model of Church et al. (2012) for the FB where unstable nuclear burning is providing part of the luminosity of flares.

Both the flare amplitudes and the flare durations have relatively small ranges. Over those ranges, the amplitudes and durations are positively and significantly correlated (see Fig. 12). The existence of this correlation suggests that the flare amplitude is not some constant 'standard candle' (as for X-ray bursts), even though the range of amplitudes is apparently fairly restricted. We do not find any significant correlation between the time between flares (either before or after) and the flare amplitude or duration. We do not have a ready explanation as to why the durations and the amplitudes get larger and smaller together over many flares.

The Sco X-1 fast optical flares have a distinct morphology, and these are definitely different from the slower brightenings and dips. The low state brightening events have durations from 0.02 to 0.10 d (30–144 min) with no overlap in duration with the high-state fast flares. These brightening events all have a smooth light curves. Their light curves are variously rounded or cuspy at the top, giving the visual impression that the peaks are formed by failed transitions between high and low states. That is, if the system conditions that determine the state are toggled over a short time interval, then dips and brightenings will be made with the light-curve variations being in the transition region between high and low states, i.e. failed state transitions. We conclude that there are two morphologically distinct types of brightening events in the Sco X-1 light curve, first the fast optical flares associated with the fast X-ray flares, and second the long-duration and smooth brightenings that are apparently failed transitions between states.

The optical high state appears to be fairly constant plateau with a flat light curve, albeit with the baseline flickering with the red noise power spectrum noted above (Scaringi et al. 2015). The fast optical flares appear to be simple additions of the flare flux on top of this plateau and are distinct from the flickering behaviour. Another manifestation of this is the break in the high-state rms–flux relation shown by Scaringi et al. (2015). The transitions to the low state make for quick fades from the high-state-plateau as well as fast rises to the plateau. Both the flares and the transitions contribute substantially to the broadening of the histograms of orbit-modulation-corrected flux for the high state. We can define a pure-optical-high state as being when Sco X-1 is optically bright, not rising or falling from a transition, and not during a fast flare. Sco X-1 is in this state about a quarter of the time. During this pure-optical-high state, the flux is still varying on fast and slow time-scales. Thus, we see some small amplitude variability that does not qualify as our fast optical flares, and we see some variations up and down in the plateau level. With all these superposed variations, nevertheless, the pure-optical-high state appears to be essentially a nearly flat plateau.

The fast optical flares *only* occur during the flat plateau of the high state. That is, we never see any fast flares in the low state, in the transition state, during small dips in the high-state plateau, or even on the edges when the transition state is merging with the high state. As already noted, and discussed further in Section 6, the high state is near synonymous with the X-ray FB in the Z-diagram. So we have equalities between events and states from the X-ray and optical light curves, where the X-ray fast flares are the same events as the optical fast flares, and the X-ray FB is identical with the optical high state. The optical fast flares are caused by the X-ray flares produced on or near the surface of the neutron star (perhaps from episodic nuclear burning), and these are only seen during the optical high state, which is to say that the X-ray flares only occur during the X-ray FB. So the branch on the Z-diagram is well named, and we are showing here with the long *Kepler* data set that the other branches do not have flares.

We have constructed a light curve of the optical high state with the fast flares included and the transitions excluded, all with the orbital modulation removed. For this, we have further normalized out the slow variations in the plateau level by picking out one or two points a day as representative of the plateau variations and using them to define a piecewise continuous light curve that can be subtracted out. The result is a nearly flattened light curve only of the optical high state with the fast flares riding on top. This light curve has been folded on the known orbital period, as shown in Fig. 13 for the first

30 d. This plot shows the sharp upper cut-off of the flare amplitudes. This also shows that this plotted flare amplitude does not change substantially with orbital phase. Recall that this plot has already been corrected for the orbital modulation by a multiplicative factor that varies sinusoidally with phase so as to flatten the light curve. Thus, the uncorrected flare amplitude must scale with the mean optical light. This is a more specific restatement of the finding in Section 3 that in the high state, the standard deviation appears to be modulated in the same way as the average light. The plot also shows that the flare frequency does not vary with the orbital phase.

6 CORRELATIONS WITH MAXI AND *FERMI* GBM

Early coordinated studies identified a pattern of correlations between X-ray and optical flux (Bradt et al. 1975; Canizares et al. 1975; Mook et al. 1975). At low optical brightnesses the X-ray emission appeared approximately constant, but above a threshold optical brightness X-rays became extremely variable and on average brighter. McNamara et al. (2003) refined the correlation using BATSE and ground-based optical fluxes, and noted an inverse relation between optical and X-ray flux at low optical brightnesses, but the data were sparse. Scaringi et al. (2015) showed the correlations between *Kepler* and MAXI exhibiting a huge improvement over earlier work, with the NB anti-correlation clear and large X-ray variability in the FB. For comparison, O'Brien et al. (2004) presented a comparable correlation for Cyg X-2, in which X-rays first increased then decreased with optical flux as the Z-diagram was traced from HB to FB. This is the *opposite* of what is observed in Sco X-1.

Our multi-wavelength data set includes two quite different subsets. The *Kepler* optical data are near-continuously sampled with gaps between exposures usually small compared to the exposure time. The GBM and MAXI data are extremely sparsely sampled and consequently do not represent well-resolved X-ray light curves. We can none the less produce pairs of matched X-ray and optical points, either obtained simultaneously, or for a given choice of lag, and these allow us to examine correlations. We show in Fig. 14 both the MAXI versus *Kepler* and GBM versus *Kepler* relations. By using MAXI scan times and GBM occultation times we can match with the optical more precisely than by using binned *Kepler* light curves. In addition, by detrending the orbital modulation we can remove some of the vertical scatter in *Kepler* data. Fig. 14 then defines the best relations yet available between optical and X-ray fluxes in Sco X-1.

The diagrams can both be clearly delineated into two regions. In the high state, we see a small increase in baseline hard X-ray flux with increasing optical brightness, and a large increase in the dispersion. In the low state, there is an anti-correlation with the hard X-ray flux increasing as the optical flux decreases. The hard X-ray dispersion also seems to increase again as optical flux decreases (by somewhat more than expected for constant fractional variability). In between the two regimes we can define a transition region, for *Kepler* fluxes around 140 000 e^{-1} s^{-1}, where both X-ray flux, and X-ray variance seem to be minimized. We can use this region to define a cut-off to separate high and low states based on optical brightness alone. It should be noted that this cut-off lies quite closely under the high state in the diagram, and so it assigns much of the transitionary data to the low state. Since the general X-ray to optical relation (i.e. an anti-correlation) is consistent below 140 000 e^{-1} s^{-1} this may be the most meaningful division to make, indicating that the low-state behaviour persists until the transition to the high state

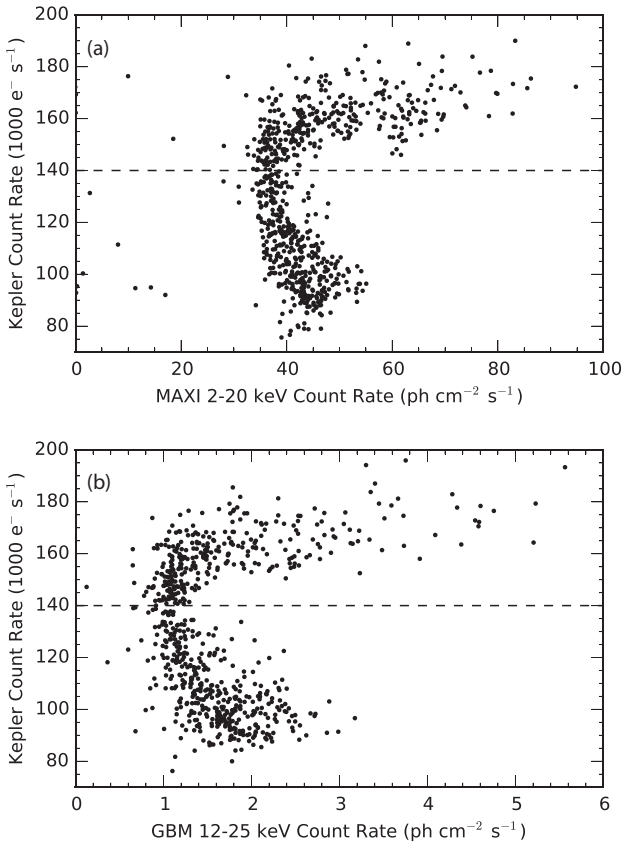

Figure 14. *Kepler* versus MAXI and GBM intensity–intensity diagrams. The dashed line indicates our division between high and low states. This figure clearly shows the low-state anti-correlation. It can be seen that the adopted dividing line corresponds to both the minimum hard X-ray flux, and the minimum X-ray variance.

is complete. This impression is also a consequence of the much steeper dependence of the optical flux on X-ray flux in the low state than the high state.

We relate optical fluxes to X-ray data in a different way in Fig. 15 where we show Z-diagrams derived from MAXI data. We highlight subsets of the data by the simultaneous optical flux. We see that the lowest optical fluxes, below the fainter of the two peaks of the optical flux histogram (Fig. 6), appear to correspond to the NB, with the upper NB almost always corresponding to very low optical fluxes. It is possible that these very low optical fluxes actually represent the HB, but this cannot be clearly identified in the MAXI Z-diagram. The intermediate-flux points between the peaks of the histogram correspond to the NB–FB transition region (the soft apex). The highest flux points correspond to the FB, and when the source is highest on the FB the optical flux is usually very high. This suggests that the optical flux increases monotonically as Sco X-1 moves from the hard apex at the top of the NB, down the NB to the soft apex, and then up the FB. We will discuss the implications of this in Section 9.

Finally, we return to the GBM versus *Kepler* flux plot and compare directly with the *Kepler* light curve. In Fig. 16 we show a segment of the light curve when the source was predominantly in the high state, with a lot of flares and some dips. GBM times of observation are overlaid at the simultaneous *Kepler* flux. We also show the X-ray/optical flux plot with the corresponding points highlighted. The flares and dips have quite distinct effects. During the flares, the X-ray flux increases strongly, loosely correlated with a moderate optical increase. During the dips the optical flux drops

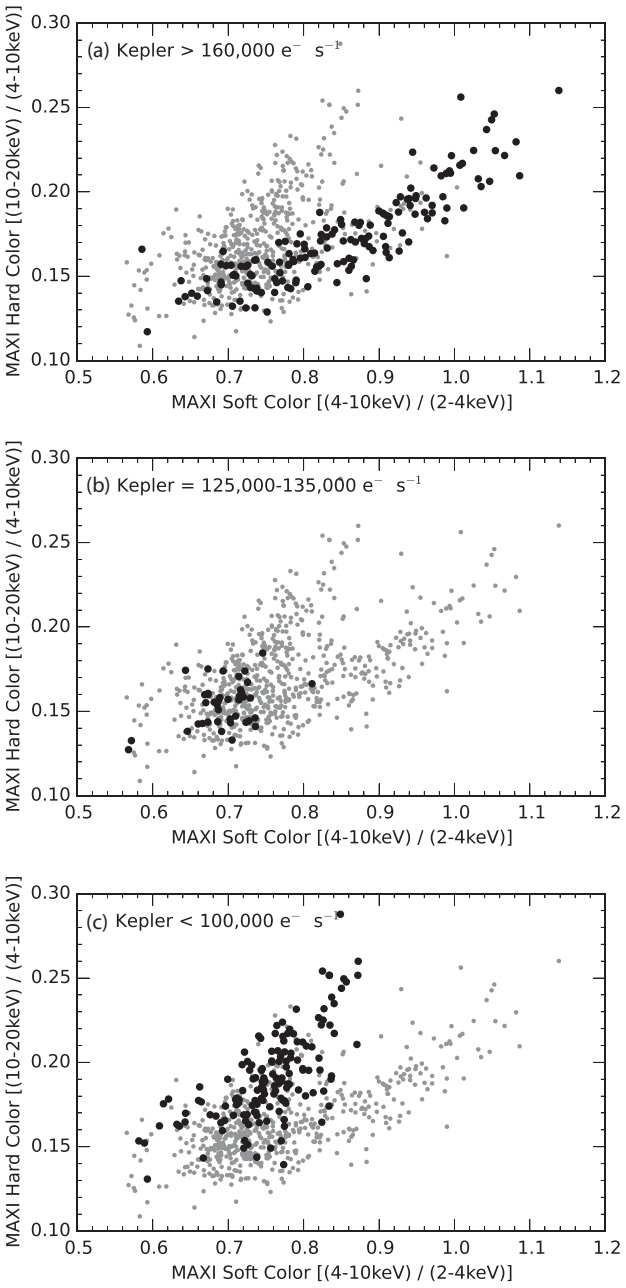

Figure 15. The MAXI Z-diagram with all data points shown in grey and optically selected points highlighted with larger solid black circles as a function of optical brightness. This shows that the optical high state corresponds to the FB and the optical low state corresponds to the NB, while optical transitions occur when Sco X-1 is at the soft apex.

substantially, with no change in X-rays or a moderate increase in X-ray flux. These changes appear to correspond to failed transitions to the low state (i.e. the NB).

We show a comparable example in the low state in Fig. 17. During this period the source was optically quite quiescent at the beginning, but there were several failed transitions to the high state towards the end. During the quiescent period at the lowest optical fluxes there are quite large variations in the hard X-ray flux. There is little corresponding optical activity and if anything an anti-correlation. The anti-correlation is more pronounced as the source moves towards the high state at the end of the segment and the hard X-ray flux decreases.

7 TIME DELAYS

Being able to match GBM and MAXI data points to single *Kepler* data points is a modest gain for the flux–flux diagrams shown in the last section but is a huge gain in constructing CCFs. We show the GBM and MAXI versus optical CCFs in Fig. 18. For MAXI we show both the combined data and energy-dependent data separately to highlight the energy dependence of the correlations. We use the discrete correlation function (DCF) of Edelson & Krolik (1988) to pair individual GBM or MAXI and *Kepler* fluxes and then bin the correlations up into 1 min bins to match the *Kepler* resolution. After removing the optical orbital modulation we subtract the mean from each light curve and then divide by the standard deviation before calculating the DCF. We follow the recommendations of White & Peterson (1994) and do not weight the individual data pairs and use the simple standard deviation for normalization rather than correcting for statistical errors.

Examining the CCFs for the combined data first, these are dominated by a sharp peak near zero lag, with a broad hump seen clearest in MAXI combined CCFs for optical lags of about 12 h. This has already been extensively discussed by Scaringi et al. (2015) and attributed to a thermal time-scale lag. These authors reinforce its significance by detection of a 12 h lag in a cepstrum analysis of the *Kepler* light curve. We reproduce this hump in all the MAXI energy bands, but not conclusively in the GBM light curve, although a weaker feature is seen at somewhat longer lags. We were able to reproduce the feature independently in subsets of the MAXI data, but a bootstrap analysis using the stationary bootstrap resampling of both the MAXI and *Kepler* data sets with the average block size set to around 2 d in both cases did not reproduce it consistently. Our analysis does not convincingly confirm or refute this feature. It may be a real, and possibly transient effect, or it may be a noise peak in the CCF.

Moving on to the CCFs selected by high or low state, we see a number of clear patterns. Generally, these are simpler than the complete CCFs. In the high state we see a generally positive correlation, while in the low state we see a dominant anti-correlation. The complete CCF will then be the residual remaining after these partially cancel each other out, so is not of great significance in itself. We therefore focus hereafter on the state-dependent CCFs. These show general trends with energy, with the higher energies tending to be simpler and stronger. The high state is dominated by a single sharp peak near zero lag. This is present at all energies, but is most sharply defined in the GBM data. In the low state, the dominant feature is an anti-correlation, also near zero lag, but broader than the high-state correlation. This appears to be strongest in higher energy data and in isolation does not appear significant in the MAXI 2–4 keV data. The low state also appears to show a broad and generally positive hump at ∼20 h lags, stronger at lower energies, but it is unclear if this is a real correlation or CCF noise. It may contribute to the broad hump in the combined CCFs.

Since the primary correlations and anti-correlations become best defined for high-energy X-ray data, we will focus on the MAXI 10–20 keV and GBM correlations in more detail. We show these in the two states in Fig. 19. We see quite good agreement between the two satellites based on independent sampling of the observation period. In the high state, the positive correlation peaks near zero lag, with formal peaks at $2.8^{+2.9}_{-2.7}$ min with respect to GBM data and $6.8^{+4.5}_{-3.9}$ min with respect to MAXI data. Uncertainties were estimated

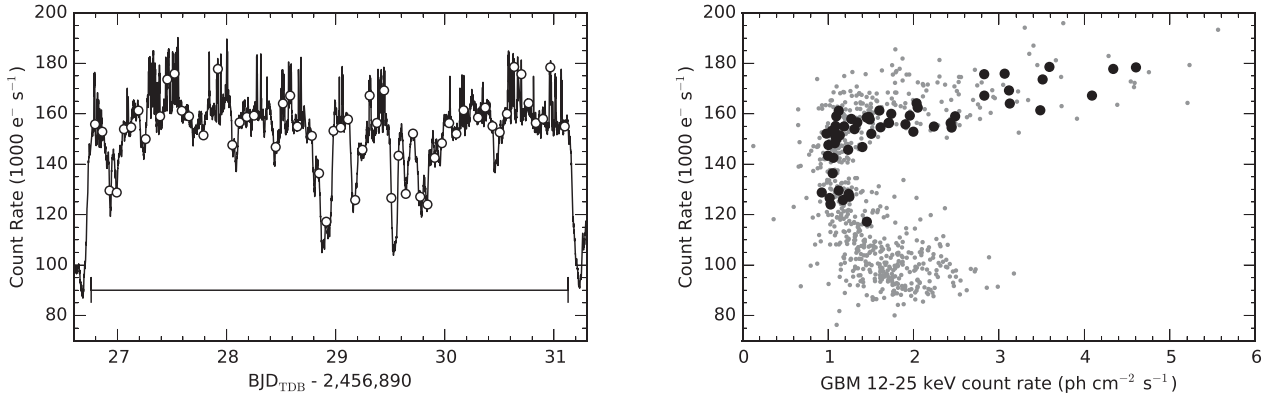

Figure 16. Left: example segment of the *Kepler* light curve when Sco X-1 was mainly in the high state with a few dips towards the low state. The horizontal bar indicates the range analysed and the open circles indicate the times of GBM occultation and the *Kepler* flux at that time. Right: *Kepler* versus GBM flux plot as in Fig. 14. All simultaneous points are shown in grey, while GBM observations from the left-hand panel are highlighted as larger black circles. Several patterns can be noted. A very small range of optical fluxes occurs on the plateau, during which the X-ray flux varies by about a factor of 2. During optical flares, the X-ray flux also increases substantially. During optical dips, the X-ray flux stays constant or slightly increases.

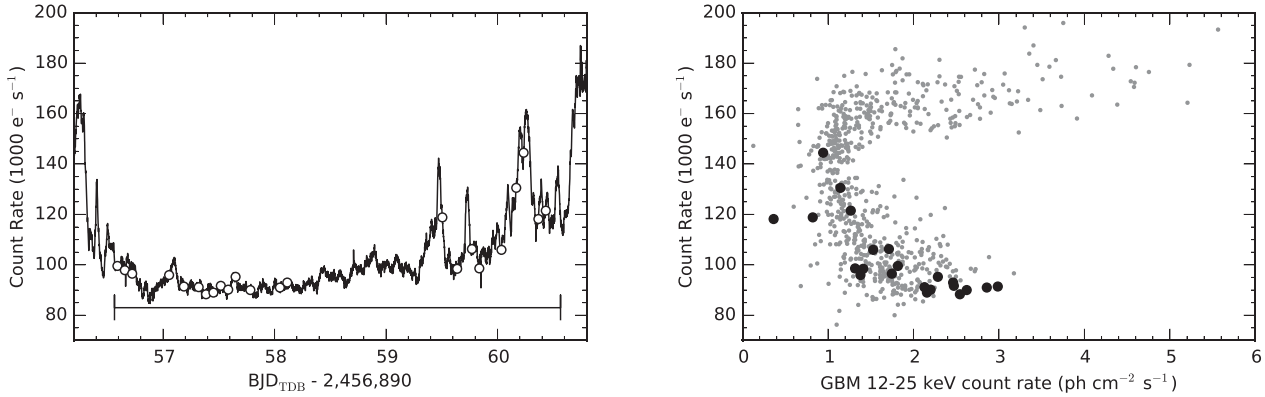

Figure 17. Left: example segment of the *Kepler* light curve when Sco X-1 was mainly in the low state with a few excursions towards the high state. Right: *Kepler* versus GBM flux plot as in Fig. 14. Notation in both plots is as in Fig. 16.

using a stationary bootstrap resampling of both the GBM/MAXI and *Kepler* data sets with the average block size set to around 2 d in both cases. The measurements suggest a modest optical lag, but do not individually rule out zero lag with high confidence. We can quantify this more formally by taking weighted averages of the lags from pairs of GBM and MAXI bootstrap lags. We find 4.8 per cent of the sample produce an average lag below zero, so zero lag can be ruled out at 95 per cent confidence, but this still leaves open the possibility that this is a coincidence with a 5 per cent probability.

In the low state, both satellites agree on the presence of a broad anti-correlation, with FWHM $\sim$ 5 h, much broader than the positive correlation in the high state (FWHM $\sim$ 25 min). The difference in widths of the features reflects the different characteristic timescales; in the high-state flares have durations of typically 5–20 min (Section 5.3), while low-state brightenings, dips, and transitions are much slower. The low-state CCF also suggests that the optical might lag the X-rays. We measure an optical lag of 29^{+30}_{-28} min with respect to the GBM data and 37^{+47}_{-43} min with respect to the MAXI data. Errors were estimated in the same way as for the high state and in this case 11 per cent of bootstrap trials yielded a weighted average of the GBM and MAXI lags below zero. Thus, although the data are consistent with quite a large lag, around 30 min, zero lag cannot be ruled out even at 90 per cent confidence.

8 STATE-DEPENDENT X-RAY SPECTROSCOPY

Using the high and low states as proxies for the X-ray FB and NB, respectively, as described in Section 6, it is possible to construct spectra of the two states as shown in Fig. 20. A third 'transition' state spectrum was created using data that were intermediate between the high and low states. MAXI data (2–20 keV)and GBM/CSPEC data (12–40 keV) were used to create the spectra. The data were separated into the appropriate states using the *Kepler* data to determine which state the source was in for a given MAXI or GBM observation and then an average spectrum was constructed for each state and each observatory. Based on the Z-diagram locations associated with optical states, we expect the high-state spectrum to be an average FB spectrum. The low-state spectrum should be an average NB spectrum, and the transition spectrum should be a spectrum at the soft apex.

The three spectra generally show more similarities than differences, reflecting the modest X-ray changes compared to the quite dramatic optical variation between states. All are dominated by a single quasi-thermal component. This is consistent with findings of other groups for the energy ranges considered (e.g. Church et al. 2012; Titarchuk, Seifina & Shrader 2014, and references therein). For example, Titarchuk, Seifina & Shrader (2014) model this quasi-thermal component as a Comptonized blackbody and find it

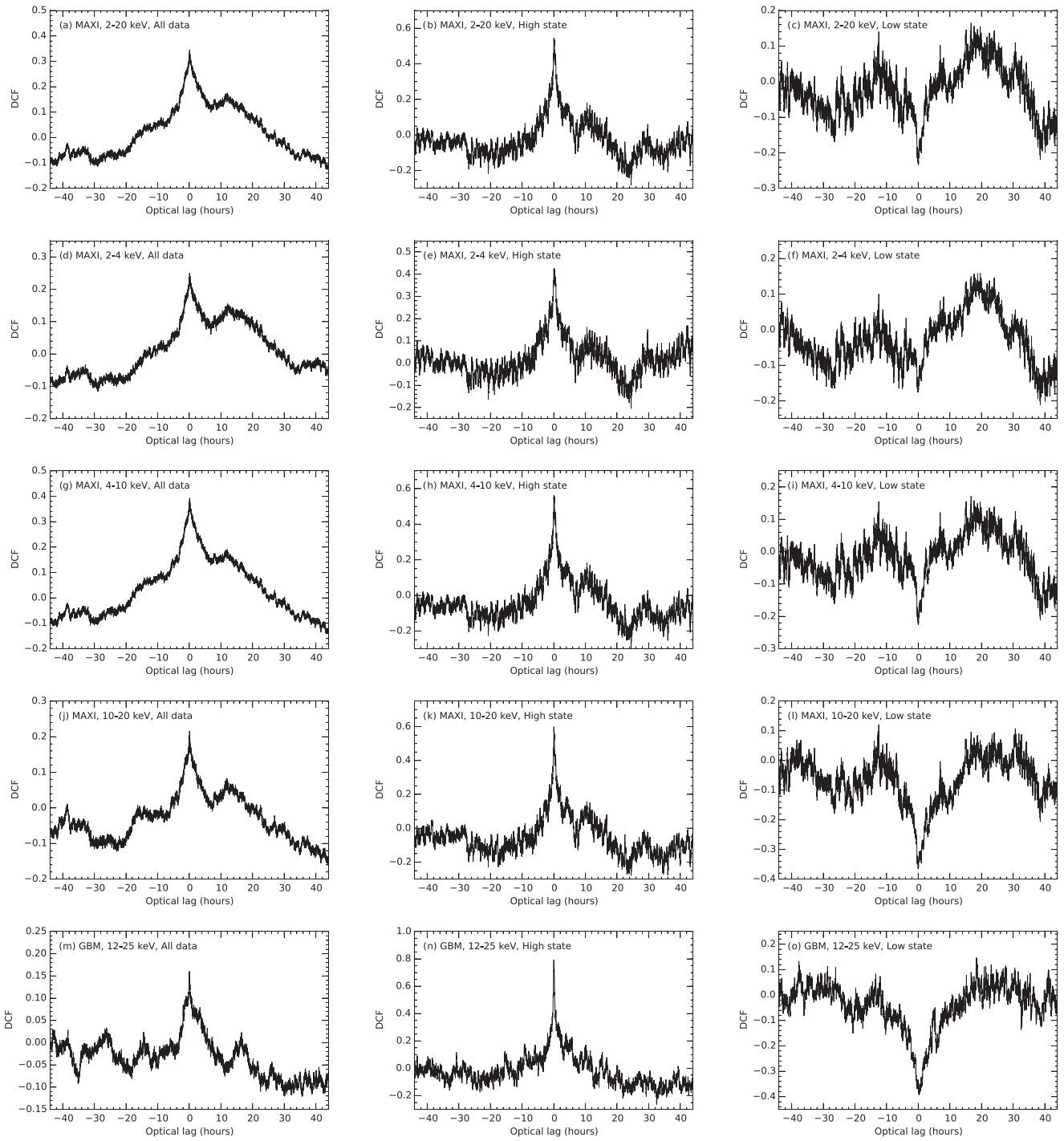

Figure 18. DCFs between MAXI or GBM and *Kepler* light curves. The left-hand panels are for the full data set, the middle panels retain only *Kepler* points from the high state, and the right hand panels retain only *Kepler* points from the low state. From top to bottom, we show correlations with the full *MAXI* data set, the *MAXI* low-energy data set, the *MAXI* medium-energy data set, the *MAXI* high-energy data set, and the full *GBM* data set. These figures clearly show distinct high- and low-state behaviour. A sharp positive correlation is always seen in the high-state data. A broader anti-correlation is always present in the low-state data, although most prominent when correlating with higher energy X-rays.

dominates the spectrum in all states below ∼40 keV. It is interpreted as blackbody emission from the neutron star surface Comptonized by hot material in the inner transition layer. Church et al. (2012) also attribute this component to the neutron star and model the spectrum as a blackbody with a cut-off power-law tail, subject to absorption.

The differences we see between the states can readily be associated with the colour changes in the Z-diagram. The optical transition state corresponds to the soft apex of the Z-diagram when the source is transitioning between NB and FB. This has the softest colours in the Z-diagram, and the lowest X-ray flux, so is the faintest state at all energies. As Sco X-1 moves up the FB (high state), its soft colour increases significantly while the hard colour only increases a little. The intensity also increases. The resulting overall higher intensity, and harder spectrum below 10 keV compared to the

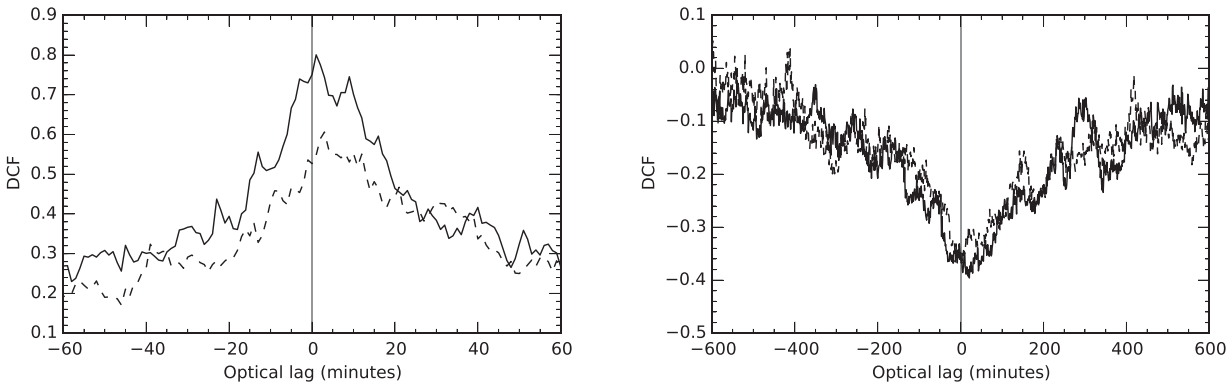

Figure 19. Expanded views of the dominant features in the GBM high-state (left) and low-state (right) CCF. Solid lines are GBM data, and dashed lines are MAXI 10–20 keV data. The vertical line indicates zero lag. These figures show that the locations and widths of the features are consistent between the two data sets.

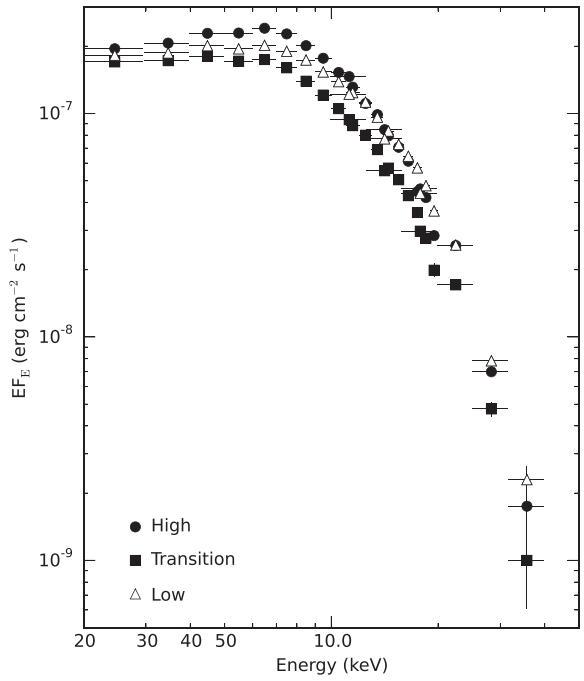

Figure 20. MAXI and GBM spectra selected according to state. Open symbols indicate MAXI data, and closed symbols are GBM data. This figure demonstrates that it is possible to use optical state classifications to separate high-energy data by state.

transition state, can readily be seen in Fig. 20. In the NB (low state), the hard colour increases more pronouncedly than the soft colour, with a less pronounced intensity change. As a result it has softer soft colours than the FB (a flatter low energy spectrum) and harder hard colours (a slower drop off at high energies), and so initially is flatter but overtakes the FB at high energies.

The spectral differences we find are entirely consistent with more comprehensive X-ray spectral analyses (e.g. Church et al. 2012; Titarchuk, Seifina & Shrader 2014, and references therein). The key innovation is that we have shown that state-dependent hard X-ray spectra can be constructed using optically defined states only. In fact, since the optical transition seen near the soft apex is quite dramatic, the optical may allow a cleaner state selection than is possible using X-ray colour–colour diagrams, though probably still inferior to a full spectral-timing classification.

9 DISCUSSION

Before attempting to tie together the results obtained, let us review the disc geometry and time-scales. For Sco X-1, assuming orbital period $P = 18.9$ h, mass ratio $q = 0.5$, and neutron star mass $M_1 = 1.4\,M_\odot$ (Mata Sánchez et al. 2015), the binary separation is about 3×10^{11} cm and the disc radius is about 1.3×10^{11} cm. Light travel time delays should then be about 10 s to the companion star and a few seconds to the disc. For typical disc edge temperatures in LMXBs (10 000–20 000 K) and temperature distributions (between $T \propto R^{-3/4}$ and $T \propto R^{-1/2}$) the V-band flux-weighted average disc radius should be about half of the total disc radius. This is about 6×10^{10} cm and should be representative of where typical optical photons originate (if they arise from thermal disc emission). At this radius we expect a dynamical time-scale, $\tau_{\rm d}$, of about 20 min (Frank, King & Raine 2002). The thermal time-scale, $\tau_{\rm th}$, should be $\tau_{\rm d}/\alpha$, where α is the viscosity parameter (Shakura & Sunyaev 1973). The α parameter can be as large as unity, although values derived in cataclysmic variables are lower, 0.1–0.4 (King, Pringle & Livio 2007). For $\alpha = 0.3$, the thermal time-scale is about 60 min at the typical optical emission radius. The viscous time-scale is much larger again, and too large to associate with the lags we measure. Even for a very large scale height of $H/R \sim 0.2$, where H is the disc half-thickness and R is the radius, we expect a viscous time-scale of around a day. For more typically assumed $H/R \sim 0.05$, the viscous time-scale becomes tens of days (comparable to the decay time-scales of outbursts of transient LMXBs; King & Ritter 1998).

Church et al. (2012) have argued that the Comptonization region responsible for the hard X-rays is not a compact inner region, but rather an extended thin, hot layer above the disc. This is supported by observations of progressive covering of the hard X-rays during X-ray dips in dipping systems, permitting an estimate of the spatial extent of the hard X-ray region. Typical estimates for the radius for the extended region are 1×10^9–7×10^{10} cm. This is at largest a factor of 10 smaller than our estimate of the radius of the region dominating optical emission, and could be much smaller than this, so even in the Church et al. (2012) model we expect the Comptonization region to be much more compact than the optical emission region, and physically distinct; it does not overlay the optical disc, for example, so in all models we expect the optical disc emission to originate from a distinct region to the X-rays.

We have shown that the optical flux generally increases as the Z-diagram is traced from hard apex to soft apex and up the FB. It has often been suggested that the optical flux may be a better tracer of mass accretion rate in Z sources than the X-ray flux is

(e.g. McNamara et al. 2003; O'Brien et al. 2004). If this is the case, then these observations vindicate the models where the Z-diagram, traced from HB to NB to FB is a monotonically increasing sequence in accretion rate (e.g. Psaltis et al. 1995). Drawing this conclusion does, however, rest on associating the optical flux with the mass accretion rate. It is far from clear that this is the case when dramatic optical changes occur on time-scales much shorter than the disc viscous time-scale. Much of the optical emission in LMXBs, in general, is attributed to reprocessing of X-ray emission (van Paradijs & McClintock 1994) and higher time resolution studies support this (Muñoz-Darias et al. 2007). We certainly see evidence for this in the variability in the FB, where good correlations are seen between X-ray and optical. Moving to the NB, however, we find no positive correlation. It is then possible that the optically emitting regions might be partially shielded from X-ray irradiation, which could result in a lower overall optical flux, even at the same or higher mass accretion rate. It is then possible that the optical flux is a poor tracer of accretion rate. This would be consistent with several more recent X-ray studies such as Church, Halai & Bałucińska-Church (2006) and Church et al. (2012), which locate the point of highest accretion rate at the hard apex where X-ray flux is maximized. Titarchuk, Seifina & Shrader (2014) also suggest that the X-ray flux should trace the accretion rate well. We will examine this possibility further in the following section.

While the peak of the CCF in the high state is marginally consistent with zero, it does suggest lags that are larger than expected from purely light travel times in the binary ($\sim$10 s). If the optical emission does arise in X-ray reprocessing there can be an additional delay due to the finite reprocessing time, dominated by the diffusion time for optical photons to reach the surface after being deposited at optical depth greater than unity. This was considered in detail by Cominsky, London & Klein (1987) who found that most of the response to X-ray irradiation should be prompt, emerging within a second, but that for reprocessing by harder photons the reprocessing time could increase substantially, with some emission continuing to a few minutes after the irradiation. This may contribute to the modest lags we see when cross-correlating with hard X-ray light curves. Strong irradiation could also lead to changes in the vertical structure of the outer disc on the thermal time-scale. Scaringi et al. (2015) invoked a thermal time-scale response to explain the $\sim$12 h lag seen with respect to MAXI data (see discussion in Section 7), although this requires lower viscosity parameters, α, than we assumed above. Given the estimates above of a thermal time-scale of about an hour, the more natural feature to associate with the disc thermal response might be the transition time-scales, with a full transition between optical states taking from one to a few thermal time-scales.

The anti-correlation in the low state is more challenging to explain. McNamara et al. (2003) and Scaringi et al. (2015) attribute the optical variability in the NB to the central region, and argue that the optical depth becomes high enough to reprocess X-ray photons to optical ones. An increase in optical depth then causes a decrease in X-rays and an increase in optical, i.e. an anti-correlation, as observed. This interpretation is also consistent with the anti-correlation being strongest at higher energies. We will discuss an alternative explanation for this in the following section.

10 AN IRRADIATIVE EXPLANATION FOR THE X-RAY/OPTICAL CONNECTIONS IN SCO X-1

We finish this work by attempting to tie together the various themes that have been discussed into a coherent picture of the relationship between X-ray and optical emission in Sco X-1. There is a long history of belief that the optical emission in luminous LMXBs such as Sco X-1 is dominated by the outer accretion disc and secondary star, and more specifically by thermal reprocessing of X-ray emission (van Paradijs & McClintock 1994). In this section, we will explore the extent to which our observations, and in particular the bimodal behaviour and anti-correlations, can still be explained within the thermal reprocessing paradigm.

We begin by returning to the *Kepler* light curve shown in Fig. 5. This, together with the flux histogram (Fig. 6), demonstrates a clear bimodal behaviour. The high state consists of a roughly flat plateau with fast flares and slower dips. The low state shows flat or U-shaped minima with slow brightenings. The low-state brightenings and high-state dips both share a common time-scale, which is also the time-scale of full state transitions. It is notably longer than the time-scales of high-state flares which appear to be a distinct phenomenon. The high-state flares involve substantial increases in X-ray flux and more modest correlated increases in optical flux. This behaviour is consistent with thermal reprocessing. As the system transitions to the low state, we see a substantial decrease in optical flux at nearly constant X-ray flux in all the energy bands studied. Quantitatively, the high-state peak in the optical histogram is at a 60 per cent higher optical flux than the low state. In contrast, depending on the energy band studied, the average X-ray flux for observations during the high state in Fig. 14 is only 10–22 per cent higher than in the low state. Furthermore, as Sco X-1 moves from the soft apex up the NB, the optical flux continues to decrease even while the X-ray flux is *increasing*; this is the X-ray to optical anti-correlation. Detailed spectral modelling by Church et al. (2012) suggests that movement away from the soft apex along the FB and the NB both involve increasing X-ray luminosity, and this conclusion is supported by Titarchuk, Seifina & Shrader (2014). The decrease in optical flux cannot then simply represent reduced X-ray luminosity, so if it arises by irradiation this must reflect a decreased irradiation efficiency in the low state (cf. Dubus et al. 1999) as a consequence of changes in either the X-ray spectral shape (and hence albedo to those X-rays) and/or illumination geometry.

A key observation here is that most of the change in optical flux during a transition (complete or failed) between the high and low states occurs at nearly constant X-ray flux (Fig. 14). X-ray data during times of optical transition are also clearly located at the soft apex of the Z-diagram, and do not significantly extend on to either the flaring or NB (Fig. 15). The transitions, therefore, do not correspond to significant changes in either the X-ray intensity or the X-ray spectrum, so cannot be explained by either luminosity or spectral shape changes. Even if spectral changes did come into play, we have shown in Section 8 that the X-ray spectral changes between high and low state are quite modest, at least from 2 to 40 keV, consistent with findings of Church et al. (2012) and Titarchuk, Seifina & Shrader (2014). It thus seems that we must look to changes in the illumination geometry to explain the optical state changes.

The overall light curve is quite suggestive of variable obscuration, with the high state and low state corresponding to minimum and maximum obscuration. The dynamic range of the material causing the obscuration may extend beyond that necessary to fully expose or fully obscure the illuminating source, leading to saturated flat maxima in the high state and, to a lesser extent, flat minima in the low state. In the clear state a partial obscuration can occur causing a dip, and in the obscured state the obscuration can partially recede creating a brightening, which is actually a reduction in the obscuration. If the Sco X-1 behaviour arises in a similar way then it is natural that the time-scales for high-state dip and low-state brightening are similar, as both arise on time-scales for changes

in the obscuration. In the case of Sco X-1 we are not suggesting that the optical light source itself is being obscured, rather that obscuration in the inner disc is blocking irradiation of the outer disc and possibly the companion. We also emphasize that we are not suggesting that the more efficient illumination in the high state causes flaring behaviour, rather that when the inner accretion flow enters its high-state configuration, two effects are seen: it becomes unstable to flaring, and it illuminates the outer disc more efficiently.

Such obscuration does arise in models of the inner disc of Sco X-1. For example, Titarchuk, Seifina & Shrader (2014) identify the dominant Comptonization region as a vertically extended transition region between the accretion disc and the neutron star. Much of the X-ray flux that we see is scattered from the inner face of this region and would not efficiently irradiate the outer disc. Equally, the extended Comptonization region above the inner disc of Church et al. (2012) would tend to scatter X-rays originating from near the neutron star and reduce direct illumination of the outer disc. Bradshaw, Geldzahler & Fomalont (2003) also invoke geometric changes in the accretion configuration between states. A variety of behaviours could produce the observed signatures. If there is a thick torus in the inner disc, for example the transition region of Titarchuk, Seifina & Shrader (2014), then decreasing the geometrical thickness of the torus would increase disc irradiation. If there is clumpy absorbing material above the disc, then decreasing the covering factor would increase irradiation of both disc and companion. If the optical depth of scattering material above the disc decreases then more direct irradiation would escape to illuminate the outer disc and companion. In any of these cases the disc could only be irradiated by a small fraction of the X-ray flux that emerges along our line of sight with the potential for large variations in the illumination as the inner disc geometry changes. Of the three examples, a torus of changing thickness would be expected to affect the disc more than the companion, leading to changes in the amplitude of the orbital modulation between states, inconsistent with observations.

It is at first puzzling that such structural changes should occur suddenly at the soft apex, rather than while ascending either the normal or FB, but there is evidence for such abrupt changes in the timing behaviour of Sco X-1. It is seen that dramatic changes in the quasi-periodic oscillation frequencies can occur with negligible movement in the Z-diagram (Dieters & van der Klis 2000), and that the bottom NB and bottom FB have nearly identical energy spectra but quite different time variability properties (Titarchuk, Seifina & Shrader 2014). As a result distinctly different normal and FB states can coexist at the soft apex for virtually the same X-ray intensity and colours. Changes in timing behaviour should reflect structural changes in the inner disc, and so could be associated with the changes in illumination geometry that we infer. The time-scales for NB–FB transitions can range from minutes for the fastest timing excursions (Dieters & van der Klis 2000) up to more typical transitions lasting tens of minutes or longer (Priedhorsky et al. 1986). These are comparable to the shortest transition time-scales that we see in the optical, but shorter than is typical. The time taken to complete a full state transition, $\sim$1.7 h rising and $\sim$2.0 h falling is quite similar to our estimates of the disc thermal time-scale, so it may be that the optical transitions also involve the disc adjusting to the change in irradiation on the thermal time-scale.

Finally, we note that extended periods of predominantly high-state behaviour last for about a week, quite comparable to the viscous time-scale estimated above. If enhanced irradiation is responsible for the changes in the high state, and leads to adjustments in the outer disc vertical structure on the thermal time-scale, we would then expect this to modulate the accretion flow through the disc. Such an accretion rate change would take approximately the viscous time to propagate to the inner disc where it could then end the predominantly high-state episode.

11 CONCLUSIONS

We have analysed *Kepler* data from the K2 mission for Sco X-1 in conjunction with simultaneous *Fermi* GBM and MAXI X-ray data. The overall light curve shows a bimodal form, with high optical fluxes when the source is on the X-ray FB and lower fluxes on the NB. During the optical high state we see a mix of fast flares and slower dips. During the low state we see slower brightenings on similar time-scales to the high-state dips. The overall impression given is that the brightenings and dips represent failed transitions between the low and high state, whereas the faster flares are distinct. We correlate the *Kepler* light curves against simultaneous *Fermi* GBM and MAXI measurements of the hard X-ray flux. We find a clear relation between hard X-ray and optical flux, with the optical positively correlated with hard X-rays in the high state and anti-correlated in the low state. This can be seen both from flux–flux diagrams, and from CCFs. We emphasize that the cross-correlation behaviour is completely different in high and low states, and so an average CCF combining states is confused and should be interpreted with caution.

There is a clear orbital modulation, consistent with earlier observations but of unprecedented quality. No compelling deviations from an average sinusoidal form are found, and neither are significant differences in the fractional amplitude of the orbital modulation between high- and low-state observations.

We have analysed the statistical distribution of several characteristic events in the light curve for which *Kepler* provides an unprecedented and uniform sample. Extended periods of predominantly high-state behaviour last for about a week, possibly being shut off by changes on the disc viscous time-scale. In more detail, uninterrupted high-state periods have a log-normal distribution with median duration of 4.7 h. There appears to be a characteristic time-scale for transitions between low and high states, with these often showing an exponential rise and decay with median times for full transitions of 1.7 h when increasing flux and 2.0 h when decreasing. The slower decay time appears statistically significant. These time-scales are common not only to full transitions, but also to partial brightenings from the low state and dips from the high state. Finally, the high-state flares show a striking uniformity of amplitude with an apparent cut-off at a maximum amplitude. The flares show no systematic asymmetry in time, and durations (typically 5–20 min) that correlate positively with the amplitude. They are likely to be produced by thermal reprocessing of the X-ray flares for which the FB is named. High-state CCFs with GBM and MAXI show a sharp positive response with delay of no more than a few minutes and marginally consistent with zero. This is consistent with the thermal reprocessing picture. A delay of a few minutes could arise from a finite reprocessing time as hard X-ray photons deposit energy at significant optical depth in the disc and companion star.

In the low state, the optical anti-correlates with X-rays, with large optical changes occurring during the transition for modest X-ray changes. Both high-state dips and low-state brightenings seem to be manifestations of failed state transitions. Deeper in the low state we see larger X-ray changes for small optical ones, but the anti-correlation is maintained. CCFs in the low state show a pronounced anti-correlation feature, most prominent with respect to GBM and to the MAXI highest energy band. The anti-correlation is much

broader than the high-state correlation and suggests a 30-min optical lag, although remains marginally consistent with zero lag.

The clear separation of states using optical data can be exploited to classify multi-wavelength data by state when other diagnostics (e.g. X-ray colour–colour diagrams, or fast X-ray timing) are not available. We demonstrate this by classifying individual GBM occultation measurements into high, low and transition states and constructing a hard X-ray spectrum for each. This is the first time this has been possible with GBM data, as they provide no sensitivity to soft X-ray colours or high-frequency variability.

We suggest that the bimodal optical behaviour is caused by changes in the efficiency with which the outer disc is irradiated with efficient irradiation in the high state and reduced irradiation in the low state. These changes could arise from increases in the thickness or covering factor of obscuring material, or increases in scattering optical depth which scatter material out of line of sight to the outer disc. The time-scales of optical transitions are comparable to, or longer than, the time-scales of transitions in X-ray timing behaviour at the soft apex of the Z-diagram. Changes in X-ray timing signatures presumably reflect changes in the accretion configuration near the neutron star, and so can be expected to affect irradiation efficiency. This then leads to dramatic changes in optical brightness when Sco X-1 transitions between the different configurations of the normal and FB possibly also involving a thermal time-scale adjustment in the outer disc vertical structure which smears out the transitions.

ACKNOWLEDGEMENTS

This paper includes data collected by the *Kepler* and *Fermi* missions. Funding for these missions is provided by the NASA Science Mission directorate. The *Kepler* data presented in this paper were obtained from the Mikulski Archive for Space Telescopes (MAST). STScI is operated by the Association of Universities for Research in Astronomy, Inc., under NASA contract NAS5-26555. Support for MAST for non-*HST* data is provided by the NASA Office of Space Science via grant NNX13AC07G and by other grants and contracts.

This work made use of PyKE (Still & Barclay 2012), a software package for the reduction and analysis of *Kepler* data. This open source software project is developed and distributed by the NASA Kepler Guest Observer Office.

This research has made use of MAXI data provided by RIKEN, JAXA and the MAXI team. We are grateful to Tatehiro Mihara for providing us with scan time data.

SS acknowledges funding from the Alexander von Humboldt foundation. We are grateful for helpful suggestions from our referee which enriched the analysis in this paper. This research has made use of NASA's Astrophysics Data System.

REFERENCES

Augusteijn T. et al., 1992, A&A, 265, 177
Bradshaw C. F., Geldzahler B. J., Fomalont E. B., 2003, ApJ, 592, 486
Bradt H. V. et al., 1975, ApJ, 197, 443
Britt C. T., 2013, PhD thesis, Louisiana State University
Canizares C. R. et al., 1975, ApJ, 197, 457
Church M. J., Halai G. S., Bałucińska-Church M., 2006, A&A, 460, 233
Church M. J., Gibiec A., Bałucińska-Church M., Jackson N. K., 2012, A&A, 546, A35
Cominsky L. R., London R. A., Klein R. I., 1987, ApJ, 315, 162
Cowley A. P., Crampton D., 1975, ApJ, 201, L65
Dieters S. W., van der Klis M., 2000, MNRAS, 311, 201
Dubus G., Lasota J.-P., Hameury J.-M., Charles P., 1999, MNRAS, 303, 139
Eastman J., Siverd R., Gaudi B. S., 2010, PASP, 122, 935
Edelson R. A., Krolik J. H., 1988, ApJ, 333, 646
Efron B., 1979, Ann. Statist., 7, 1
Fomalont E. B., Geldzahler B. J., Bradshaw C. F., 2001, ApJ, 558, 283
Frank J., King A., Raine D. J., 2002, Accretion Power in Astrophysics. Cambridge University Press, Cambridge, UK
Galloway D. K., Premachandra S., Steeghs D., Marsh T., Casares J., Cornelisse R., 2014, ApJ, 781, 14
Gandhi P., 2009, ApJ, 697, L167
Giacconi R., Gursky H., Paolini F. R., Rossi B. B., 1962, Phys. Rev. Lett., 9, 439
Gottlieb E. W., Wright E. L., Liller W., 1975, ApJ, 195, L33
Hakala P., Ramsay G., Barclay T., Charles P., 2015, MNRAS, 453, L6
Hasinger G., van der Klis M., 1989, A&A, 225, 79
Hiltner W. A., Mook D. E., 1967, ApJ, 150, 851
Hiltner W. A., Mook D. E., 1970, A&A, 8, 1
Hjellming R. M., Johnston K. J., 1981, ApJ, 246, L141
Homan J. et al., 2010, ApJ, 719, 201
Howell S. B. et al., 2014, PASP, 126, 398
Hynes R. I., Britt C. T., 2012, ApJ, 755, 66
Ilovaisky S. A., Chevalier C., White N. E., Mason K. O., Sanford P. W., Delvaille J. P., Schnopper H. W., 1980, MNRAS, 191, 81
King A. R., Ritter H., 1998, MNRAS, 293, L42
King A. R., Pringle J. E., Livio M., 2007, MNRAS, 376, 1740
Koch D. G. et al., 2010, ApJ, 713, L79
Künsch H. R., 1989, Ann. Statist. 17, 1217
Lin D., Remillard R. A., Homan J., 2009, ApJ, 696, 1257
Lin D., Remillard R. A., Homan J., 2010, ApJ, 719, 1350
Liu R. Y., Singh K., 1992, in LePage R., Billard L., eds, Exploring the Limits of Bootstrap. John Wiley, New York, p. 225
Lyubarskii Y. E., 1997, MNRAS, 292, 679
Maccarone T. J., 2002, MNRAS, 336, 1371
McGowan K. E., Charles P. A., O'Donoghue D., Smale A. P., 2003, MNRAS, 345, 1039
McNamara B. J. et al., 2003, AJ, 125, 1437
Mata Sánchez D., Muñoz-Darias T., Casares J., Steeghs D., Ramos Almeida C., Acosta Pulido J. A., 2015, MNRAS, 449, L1
Matsuoka M. et al., 2009, PASJ, 61, 999
Mook D. E. et al., 1975, ApJ, 197, 425
Muñoz-Darias T., Martínez-Pais I. G., Casares J., Dhillon V. S., Marsh T. R., Cornelisse R., Steeghs D., Charles P. A., 2007, MNRAS, 379, 1637
O'Brien K., Horne K., Hynes R. I., Chen W., Haswell C. A., Still M. D., 2002, MNRAS, 334, 426
O'Brien K., Horne K., Gomer R. H., Oke J. B., van der Klis M., 2004, MNRAS, 350, 587
Petro L. D., Bradt H. V., Kelley R. L., Horne K., Gomer R., 1981, ApJ, 251, L7
Politis D. N., Romano J. P., 1994, J. Am. Stat. Assoc., 89, 1303
Priedhorsky W., Hasinger G., Lewin W. H. G., Middleditch J., Parmar A., Stella L., White N., 1986, ApJ, 306, L91
Psaltis D., Lamb F. K., Miller G. S., 1995, ApJ, 454, L137
Sandage A. et al., 1966, ApJ, 146, 316
Scaringi S., Maccarone T. J., Hynes R. I., Körding E., Ponti G., Knigge C., Britt C. T., van Winckel H., 2015, MNRAS, 451, 3857
Shakura N. I., Sunyaev R. A., 1973, A&A, 24, 337
Steeghs D., Casares J., 2002, ApJ, 568, L273
Still M., Barclay T., 2012, ascl.soft, 1208.004
Titarchuk L., Seifina E., Shrader C., 2014, ApJ, 789, 98
Uttley P., McHardy I. M., Vaughan S., 2005, MNRAS, 359, 345
van Paradijs J., McClintock J. E., 1994, A&A, 290, 133
Vrtilek S. D., Penninx W., Raymond J. C., Verbunt F., Hertz P., Wood K., Lewin W. H. G., Mitsuda K., 1991, ApJ, 376, 278
White R. J., Peterson B. M., 1994, PASP, 106, 879
Wilson-Hodge C. A. et al., 2012, ApJS, 201, 33

This paper has been typeset from a TEX/LATEX file prepared by the author.